Switching Extensional and Contractional Tectonics in the West Kunlun Mountains During Jurassic: Responses to the Neo-Tethyan Geodynamics along the Eurasian Margin

Hong-Xiang Wu[1,2], Han-Lin Chen[1,2*], Andrew V. Zuza[3], Yildirim Dilek[4], Du-Wei Qiu[1,2], Qi-Ye Lu[1,2], Feng-Qi Zhang[1,2], Xiao-Gan Cheng[1,2], Xiu-Bin Lin[1,2]

1 School of Earth Sciences, Zhejiang University, Hangzhou, China.

2 Structural Research Center of Oil & Gas Bearing Basin of Ministry of Education, Hangzhou, China.

3 Nevada Bureau of Mines and Geology, Nevada Geosciences, University of Nevada, Reno, NV, USA.

4 Department of Geology & Environmental Earth Science, Miami University, Oxford, OH, USA.

ORCID: 0000-0003-4997-8715 (Hong-Xiang Wu)

*Corresponding author: hlchen@zju.edu.cn (Han-Lin Chen)

Address: No. 1 Hainayuan Building, Zijingang Campus, Zhejiang University, 866 Yuhangtang Road, Hangzhou, Zhejiang, P.R. China.

Submitted to: Solid Earth

Abstract: The Tethyan Orogenic Belt records a long-lived geological cycle involving subduction and collision along the southern margin of the Eurasian continent. The West Kunlun Mountains, located at the junction between the Tibetan and Western Asian Tethyan realm, records multiple orogenic events from the Paleozoic to the Cenozoic that shape the northwestern Tibetan Plateau. However, deciphering the complex Mesozoic contractional and extensional tectonics to interpret the broader Tethyan geodynamics remains challenging. To address the tectonic transition following the early Cimmerian (Late Triassic) collision, this study investigates the newly identified Jurassic sedimentary strata and volcanic rocks in the West Kunlun Mountains. Zircon geochronological results of basalts and sandstones reveal that this ~ 2.5-km-thick package was deposited at ca. 178 Ma, rather than the previously reported Neoproterozoic age. The alkaline basalts at the top of the formation exhibit chemical compositions similar to oceanic island basalts, consistent with the intracontinental extension environment revealed by the upward-fining sedimentary pattern. Provenance analysis, integrating conglomerate clast lithologies with detrital zircons, suggests a substantial contribution from adjacent basement sources, likely influenced by the normal faulting during initial rift stage. These findings indicate that the West Kunlun Mountains rapidly transitioned into an extensional setting after suturing with Cimmerian terranes. The regional structure, stratigraphy and magmatism suggest that this Early - Middle Jurassic basin was subsequently inverted during the Late Jurassic and earliest Cretaceous. We propose that the Mesozoic deformational history in the West Kunlun Mountains was related to the northward subduction of the Neo-Tethys Ocean, as it transitioned from southward retreat to northward flat-slab

advancement. Comparing with the entire strike-length of the Eurasian Tethyan orogen, we find that the subduction mode varied from the west to the east, reflecting the broad geodynamic changes to, or initial conditions of, the Neo-Tethyan system.

Keywords: Tethyan Orogenic Belt; West Kunlun Mountains; Jurassic volcanics; Basin evolution; Subduction retreating and advancing.

1 Introduction

The Tethyan Orogenic Belt, a trans-Eurasian mountain system spanning an east-west strike-length of over 15,000 km, is characterized by a series of mountain chains and orogenic plateaus along its latitudinal extent (Fig. 1a; Şengör, 1987; Metcalfe, 2013; Wu et al., 2020). The evolution of the Tethyan Orogenic Belt involved multiple phases of ocean basin opening and closing (i.e., the Proto-, Paleo-, and Neo-Tethys oceans) throughout the Phanerozoic era, which resulted in the development of multiple orogenic belts across the Eurasian continent (Stampfli, 2000; Wan et al., 2019; Metcalfe, 2021). The complex history of accretionary and collisional orogenesis in the Tethyan realm is intricately linked to the breakup and formation of the two mega-landmasses, Gondwana and Laurasia (Şengör et al, 1988; Stampfli and Borel, 2002; Zuza and Yin, 2017; Li et al., 2018; Wang et al., 2018). Documenting the mode and nature of the accretionary and collisional events in the Mesozoic history of the Tethyan orogenic system is, therefore, important for understanding the continental dynamics of Eurasia.

The Mesozoic Tethyan Orogenic Belt involved a protracted phase of orogenesis, rifting, and basin evolution, associated with the convergence between the southern Asian margin and Cimmerian terranes derived from Gondwana (e.g., Kazmin, 1991; Stampfli and Borel, 2002; Angiolini et al., 2013; Robinson, 2015). The tectonic evolution of the Tethyan realm during the Mesozoic exhibits significant variations from the west to the east (Şengör, 1984; Zhu et al., 2022). In the Western Asian section of the Tethyan Orogenic Belt, geochronological and geochemical data from diverse magmatic rocks assemblages suggest a propagating continental rift system in the southern

margin of the Iran Block during the Early Jurassic to Early Cretaceous (Hunziker et al., 2015; Lechmann et al., 2018; Azizi and Stern, 2019). This process is envisioned to have been associated with subduction geodynamics involving multiple intraoceanic subduction zones, slab tearing, and alternating slab rollback and advance within Neo-Tethys (Zhang et al., 2018; Jafari et al., 2023). Conversely, in the Eastern Asian section of the Tethyan Orogenic Belt (i.e. Tibetan sector), an Andean-type orogeny along the southern margin of Eurasia from the Early Jurassic to the Early Cretaceous has been proposed to explain deformation and sedimentation patterns in the southern Tibetan Plateau (Kapp et al., 2007; Zhang et al., 2012; Xie and Dilek, 2023). This process was punctuated by Toarcian-Aalenian back-arc rifting event resulting from retreat of the subducting Neo-Tethyan seafloor (Hou et al., 2015; Wei et al., 2017).

The West Kunlun Mountains, stretching from the northern Pamir to northwestern Tibetan Plateau, occupy a critical position at the junction between the western and eastern Tethyan Orogenic Belts (Fig. 1b; Şengör, 1984; Wu et al., 2016). The Kunlun Mountains involved the closure of the Paleo-Tethyan Ocean in the Triassic-Jurassic, followed by Cenozoic deformation and uplift during the Himalayan orogeny (Mattern and Schneider, 2000; Cao et al., 2015; Li et al., 2019; Xiao et al., 2002). Hence, the Mesozoic geology of the West Kunlun Mountains documents the plate tectonic history of the junction region within the Tethyan realm, providing pivotal insights into the formation of this extensive orogenic system. In particular, the Cimmerian Orogeny in the West Kunlun region critically represents the collision between the Gondwana- derived continental fragments and the southern Eurasian margin in the latest Triassic to late Jurassic (e.g., Şengör, 1979), but the timing and duration of this orogen

remains equivocal. Existing interpretations of the Jurassic palaeogeography and evolution vary, ranging from syn-orogenic (Cao et al., 2015), post-orogenic (Wu et al., 2021), to transtensional (Sobel, 1999), because of the scarcity of the relevant geological record from this period. Significant challenges also persist in understanding the Mesozoic evolution of the Pamir terranes (Angiolini et al., 2013), including the timing of suturing and exact kinematics of related deformation (Robinson, 2015). The Cenozoic contractional deformation episodes, due the northward subduction of the Neo-Tethyan Ocean and the collision of India with Eurasia, further complicates our understanding in this remote region (Burtman and Molnar, 1993; Cowgill, 2010). The limited knowledge of the Jurassic and Cretaceous evolution of the Pamir interior has been preliminarily deduced from the timing and nature of regional magmatic activities (Chapman et al., 2018) that are challenged by the information derived from the surrounding, fragmented sedimentary basins (Leith, 1985; Wu et al., 2021).

To better understand the regional evolution and tectono-magmatic processes in the West Kunlun Mountains, we have undertaken a systematic geochronological and geochemical study and detailed analyses of sedimentary provenance of volcaniclastic rock suites in a Jurassic basin. By integrating these new results with existing data from the adjacent region, this study provides further constraints on the Mesozoic tectonic history of the central junction of the Tethyan Orogenic Belt, probing the preceding processes that cause the formation of the broad plateau in central Asia.

2 Geological framework and sampling

2.1 Tethyan history

The Tethyan Orogenic Belt is a vast, east-west-extending mountain system that separates the main Eurasian cratons and stable platforms in the north from Gondwana - derived continental terranes in the south (e.g., Şengör et al, 1988; Stampfli et al., 1991). The development of the Tethyan Orogenic Belt involves the evolution of multiple ocean basins and their seaways, including the Proto-Tethys, Paleo-Tethys, and Neo-Tethys (Stampfli, 2000; Metcalfe, 2021). These ancient ocean basins overlapped in time but closed successively as the Gondwana - derived ribbon continents (i.e., Apulia, Pelagonia, Sakarya, Tauride, South Qiangtang and North Qiangtang and Lhasa) accreted to the southern margin of Eurasia, creating several sub-parallel suture zones stretching from the circum-Mediterranean region, Caucasus, Iranian Plateau, and continuing eastward into the Tibetan Plateau and Southeast Asia (Fig. 1a; Dilek and Moores, 1990; Wu et al., 2020; Metcalfe, 2021).

The Cenozoic indentation of the Pamirs fundamentally affected the deformation pattern of the Tethyan Orogenic Belt and geographically divided the belt into western and eastern sectors (Tapponnier et al., 1981). The history of the Proto-Tethys was linked to the breakup of the Rodinia supercontinent (Zhao et al., 2018). The western segment of the Proto-Tethys has been defined as a Cambrian-Silurian ocean existing between Baltica and Gondwana, whereas the eastern Proto-Tethys appears to have been closed earlier in the Early Silurian, as a series of Asian blocks collided onto the northern margin of Gondwana (e.g., Stampfli and Borel, 2002). The opening of the Paleo- and Neo-Tethyan ocean basins was related to slab pull forces that caused the

detachment of the Hun (including the Tarim, North and South China) and Cimmerian terrane ribbons from the northern margin of Gondwanaland, respectively (Stampfli and Borel, 2002; Ruban et al., 2007). These terranes were successively transferred northward to the Eurasian continent, causing the closure of these internal seaways during the Cimmerian and Himalayan orogenies at the end of the Triassic and the beginning of the Cenozoic, respectively (Dilek and Furnes, 2019; Wan et al., 2019).

The final demise of the Paleo-Tethyan Ocean and the initiation of subduction in the Neo-Tethyan Ocean occurred simultaneously in the Triassic - earliest Jurassic, which is of vital importance for comprehension of the cyclical Tethyan evolution (Wan et al., 2019). The West Kunlun Mountains, situated to the north of the Pamir syntaxis, forms the western extent of the Tibetan Plateau (Fig. 1b-c). They constitute an important spatial link between the western and eastern domains of the Tethyan Orogenic Belt. The formation of the West and East Kunlun Mountains, involved accretionary and collisional orogeneses during the closure of the Proto-Tethys and Paleo-Tethys oceans (Mattern and Schneider, 2000; Xiao et al., 2005; Dong et al., 2018). The East Kunlun Mountains are deflected to the north relative to the West Kunlun Mountains by the dextral Altyn-Tagh strike-slip fault (Fig. 1b). During the Early Paleozoic, the closure of the Proto-Tethys Ocean led to the collision of the Tarim Craton (North Kunlun) and the South Kunlun terrane along the Kudi suture zone (Fig. 1c; Zhang et al., 2019a). After splitting from eastern Gondwana in the Devonian - Carboniferous, the Tianshuihai - Qiangtang blocks travelled northward towards the Tarim Craton because of the subduction of the Paleo-Tethyan Ocean floor. These blocks ultimately collided with the Tarim Craton at the latest Triassic,

forming the Mazar - Kangxiwa suture zone (Fig. 1c; Xiao et al., 2005; Metcalfe, 2021). The Pamir terranes (including the Central Pamir, South Pamir, and Karakoram), commonly regarded as the western counterpart of the Qiangtang block, rifted from Gondwana much later, during the Permian (Robinson, 2015; Angiolini et al., 2015). The major Cimmerian orogenic unconformity between the Lower Jurassic and the deformed Upper Triassic strata is generally considered to mark the timing of the integration of these Pamir terranes onto the Eurasian margin (Angiolini et al., 2013; Li et al., 2022b).

The mid-Mesozoic tectonic evolution of the West Kunlun Mountains and Pamir is somewhat enigmatic, as the first-order geodynamic mechanisms for widespread observed deformation remain unclear. Several major exhumation events, including the Late Triassic and Early Jurassic, Middle-Late Jurassic, Early Cretaceous, and Late Cretaceous, are documented by low-temperature thermochronology in the mountain ranges and surrounding basins (Sobel, 2013; Cao et al., 2015; Li et al., 2019, 2023). Mid-Cretaceous granitoid plutons are widespread in the South Pamir and Karakoram. A polymetamorphic Jurassic and Cretaceous history of the mountains is also displayed by monazite ages (Faisal et al., 2014). The basement cooling as well as magmatic, and metamorphic events have previously been interpreted as associated with far-field stress effects of collisional events (Yang et al., 2017) or a high-flux event during an Andean-type subduction of the Neo-Tethyan Ocean (Chapman et al., 2018). These Mesozoic structures within the orogenic belts were intensely reworked by the Cenozoic deformation during the Himalayan orogeny (Burtman and Molnar, 1993).

2.2 Regional geology and sampling strategy

This study focused on the central and southern parts of the northwest-trending Jurassic basin within the West Kunlun Mountains (Fig. 1c). The Kyzyltau region, situated in the central part of this Jurassic basin, preserves the thickest Early-Middle Jurassic strata. It mainly comprises the Lower Jurassic Shalitashi and Kangsu formations, and the Middle Jurassic Yangye and Taerga formations (Fig. 2a). The Shalitashi Formation comprises a massive, thick conglomerate that overlies the deformed Carboniferous and Permian shallow marine clastic rocks and limestones along an angular unconformity (Fig. 3a). The poorly sorted textures and lateral thickness variations in the conglomerate indicate that its clastic material originated from alluvial fans (Sobel, 1999; Fig. 3b-e). The Kangsu and Yangye formations form the main part of the Jurassic strata (Fig. 2a), with total stratigraphic thickness exceeding 1800 meters. The Kangsu Formation mainly comprises stacked greywackes interbedded with coal layers. The Yangye Formation consists mainly of interbedded sandstones and shales exhibiting typical Bouma sequences, indicative of turbidite deposits in a deepwater environment (Wu et al., 2021). The Middle Jurassic Taerga Formation is only exposed in the northeastern side of the region and consists of thinly-bedded shales and siltstones. The Lower to Middle Jurassic stratigraphy forms an upward-fining sequence, indicating the expanding and deepening of the basin over time. Structurally, the Jurassic strata exhibit strong deformation, forming a northwest-trending synclinorium (Fig. 2a). The Cenozoic contraction in the region extensively deformed the coal-bearing strata, resulting in the formation of multi-scale folds and thrusts (Fig. 3f and 3g). Regionally, the Early-Middle Jurassic strata are unconformably overlain by the Late Jurassic

Kuzigongsu Formation and the Cretaceous Kezilesu Group, which are characterized by oxidation-colored, massive conglomerate and sandstones (Fig. 3h). Synchronous unconformities also exist in the South Qiangtang and Bangong-Nujiang suture zones (Ma et al., 2017, 2018). This event was generally interpreted to have been linked to the Middle - Late Jurassic, large-scale contraction and aridification across central Asia (Hendrix et al., 1992; Yang et al., 2017).

Documentation and study of the Mesozoic stratigraphy in the southernmost part of the Jurassic basin have been relatively insufficient. In the Kandilik region, geological mapping identified a coal-bearing formation, known as the Lower - Middle Jurassic Yarkant Formation, and a massive conglomerate classified as the Upper Jurassic Kuzigongsu Formation (Fig. 2b). These Jurassic strata were strongly deformed and laterally bounded by a mylonitic shear zone to the west and thrust faults to the east. A stratigraphic unit of gray-black slate interbedded with fine sandstones and siltstones is exposed to the east of the Yarkant Formation, with a thickness exceeding 3500 meters (Ma et al., 1991). Abundant mafic dykes intruded into the lower part of the strata (Fig. 3i), causing local contact metamorphism. A suite of volcanic strata composed of several basalt layers are juxtaposed with the thick clastic package along a steeply-dipping fault. Several eruptive episodes are identified within this unit based on alternating volcanic horizons, including volcanic breccia (Fig. 3j), amygdaloidal basalts, and massive basalts (Fig. 3k). These volcanic rocks belong to the part of upper member deposited above the thick clastic strata (Ma et al., 1991). Due to the lack of reliable constraints from chronological results, this stratigraphic unit has long been thought as Precambrian in age (Ma et al., 1991). Structurally,

the strata were intensely deformed by regional Kashgar-Yecheng transfer faults (Fig. 2) and bedding dips steeply to the northeast (Fig. 3l).

In the Kandilik region, one basalt sample (AYBL09) was collected near the thrust fault for geochronological dating (Fig. 2b). Six fresh, undeformed basalt samples were also obtained away from faults for geochemical analysis. These basaltic rock samples consist primarily of plagioclase with a fine columnar texture and anhedral Ti-Fe oxides (Fig. 3m). Plagioclase is locally altered into chlorite. Additionally, one quartz-lithic sandstone sample (AYBL13) was collected for detrital zircon age analysis. This sample exhibits poor sorting and is composed mainly of quartz (~ 30%) with angular shapes, feldspar (<10%), and lithic fragments (> 60%) (Fig. 3n). For regional comparison, two sandstone samples were collected from the Kangsu (KZLT1601) and Yangye formations (KZLT1602) in the Kyzyltau region (Fig. 2a). These sandstones show similar textures and compositions to the clastic sample from the Kandilik region (Fig. 3o).

3 Methodology

One basalt sample (AYBL09) was collected from the Kandilik region for zircon U‐Pb geochronology and in-situ trace element analysis. Zircon separation and cathodoluminescence (CL) imaging were done at Yuheng Rock & Mineral Technology Service Co., LTD., Langfang, China. Zircons were analyzed for U‐Pb geochronology using an Agilent 8900 ICP-QQQ equipped with an ESI New Wave NWR 193UC (Two Vol2) laser ablation system at Beijing Quick-Thermo Science & Technology Co., Ltd, China. Concordia plots were constructed using IsoplotR (Vermeesch, 2018).

281 To analyze the petrogenesis and tectonic setting of magmatism, six fresh
282 basalt rocks were collected from the same section for determining their major
283 and trace element chemistry. Samples were first crushed, and powdered in an
284 agate mill. Elemental analyses were conducted at Wuhan SampleSolution
285 Analytical Technology Co., Ltd. Major-element analyses were performed by X-
286 ray fluorescence spectrometry (ZSXPrimusII), with analytical uncertainties
287 generally better than 1%. Trace-element contents were determined using an
288 Agilent 7700e ICP-MS.
289 To compare the detrital age patterns and sedimentary provenance, we
290 have conducted zircon U-Pb dating on two sandstones (KZLT1601 and KZLT1602)
291 exposed in the Kyzyltau section, and one sandstone (AYBL13) exposed in the
292 Kandilik section (Fig. 2B). Zircons from samples KZLT1601 and KZLT1602 were
293 analyzed for U‐Pb geochronology using a Thermofisher iCAP RQ ICP-MS
294 equipped with a Cetea Analyte HE laser ablation system at School of Earth
295 Sciences, Zhejiang University. Zircons from sample AYBL13 were analyzed for
296 U‐Pb geochronology using an Agilent 8900 ICP-QQQ equipped with an ESI
297 New Wave NWR 193UC (Two Vol2) laser ablation system at Beijing Quick-
298 Thermo Science & Technology Co., Ltd. The Common Pb was corrected with
299 the method proposed by (Andersen, 2002). Concordia plots and Kernel Density
300 Estimate (KDE) plots were constructed using IsoplotR (Vermeesch, 2018) and
301 Density Plotter 8.5 (Vermeesch, 2012), respectively.
302 The details of the analytical procedures and the information of the
303 analytical methodologies, as explained above, are presented in Table S1.
304 The data from the conglomerate in the Shalitashi Formation were collected
305 at eight different sections. Analysis of conglomerate clasts was conducted

within a designated 1 square meter area. Our focus was on documenting the lithological compositions of the clasts, with at least one hundred gravels randomly counted at each site.

4 Analytical Results

4.1 Morphology and geochronology of zircons from basalt samples

The results of zircon U-Pb dating of the basalt sample are presented in Table S2. Approximately one hundred and seventy zircon grains have been successfully separated from the basalt sample. Zircon crystals are mostly transparent and colorless, displaying varying lengths ranging between 50-200 μm with elongation ratios of 1:1-5:1 (Fig. 4). Upon examination of their cathodoluminescence (CL) images, we have sub-categorized these zircons into two groups based on the presence of oscillatory zoning. The grains showing well-defined growth zoning (type 1) are generally sub-euhedral in shape (no.3 in Fig. 4), which imply their magmatic origin (Fig. 4; Hoskin and Schaltegger, 2003). Another type (type 2) of zircon displays inconspicuous zoning texture (no.4 in Fig. 4) or yields only faintly visible zoning patterns (no.15 in Fig. 4). Morphological analysis of these zircons reveals a range from needle-shaped and elongated crystals (no.13 in Fig. 4) to stubby and equant forms (no.12 in Fig. 4). A common feature of these varying grains is their subrounded external appearance. This may result from moderate resorption either during the evolution of the magma chamber when the magma is oversaturated with respect to zircon or a certain degree of metamorphism (Corfu et al., 2003). In addition to their "polished" shape, these zircons commonly display nebulous or patchy-zoned centers, without distinct core-rim structures (no.11-13 in Fig. 4).

We have conducted a total of thirty-six spot analyses on various types of zircons (Fig. 4), resulting in thirty-three analyses with a > 90% concordance (Fig. 5a). The Th/U ratios of all tested zircons range from 0.04 to 1.52 (Fig. 5d). We cannot assert that all of them are primary crystals without modification simply based on the evaluation of Th/U ratios. However, all of these results yielded concordant ages spanning a broad range from the Early Neoproterozoic to the Jurassic. Type 1 zircon grains have Th/U ratios ranging from 0.38 to 1.44, while type 2 zircon grains exhibit a wider range. Based on the classification and statistical analysis of zircon characteristics, we found that type 1 zircons, which commonly exhibit clear oscillatory zoning, have older $^{206}Pb/^{238}U$ ages ranging from 405 Ma to 911 Ma, whereas type 2 zircons display uniform ages between 168 Ma and 193 Ma (Table S2). Twenty youngest zircons with the concordant ages define a weighted mean $^{206}Pb/^{238}U$ age of 178±2 Ma (MSWD = 0.99) (Fig. 5b). We interpret this Toarcian age as the crystallization age of the zircons in this rock sample. The remaining older zircons yield primarily middle Paleozoic and Neoproterozoic ages, which we interpret as inherited from the country rock.

4.2 Detrital zircon U–Pb ages from Jurassic sandstone

The zircon U-Pb geochronological dataset for the detrital zircons is presented in Table S2. A total of 101 spot analyses were conducted on zircon grains from sample AYBL13. After filtering grains with greater than 10% age discordance, 98 of them met the criteria for inclusion in the Kernel Density Estimate (KDE) visualization (Fig. 6a). The analyzed results reveal that the Th/U ratios of most effective zircons range between 0.12 and 2.61, with only four zircons yielding extremely low values below 0.1 (Fig. 5d). The results

suggest that most detrital zircons from sample AYBL13 are of igneous origin (Belousova et al., 2002). The youngest zircon grain from this sandstone yielded an apparent $^{206}Pb/^{223}U$ age of 429 ± 5Ma, whereas the oldest grain has revealed an apparent $^{206}Pb/^{207}Pb$ age of 3080 ± 22 Ma. The KDE plot reveals four main age populations with peaks at approximately 446 Ma, 820-955 Ma, 1553 Ma, and 2484 Ma (Fig. 6b).

For analyzing regional detrital provenance, two Jurassic samples from Kyzyltau were analyzed for age comparison. The Early Jurassic sample KZLT1601 underwent one hundred spot analyses on randomly selected zircon grains. These measured grains exhibit Th/U ratios ranging from 0.09 to 1.49 (Fig. 5d), consistent with an igneous origin. Eighty-nine zircon ages were plotted on or near the concordant curve (Fig. 6c), providing zircon ages ranging from 369 ± 6 Ma to 3314 ± 15 Ma. The detrital age spectrum was obtained using the KDE method and revealed similar peaks at approximately 444 Ma, 807 Ma, 1823 Ma, and 2566 Ma (Fig. 6d).

Similarly, one hundred zircon grains from the Middle Jurassic sample KZLT1602 exhibit characteristics indicative of a magmatic origin, with high Th/U ratios ranging between 0.11 and 2.63 (Fig. 5d). Ninety - eight concordant results display consistent age population with the sample KZLT1601, ranging from 345 ± 4 Ma to 3029 ± 15 Ma (Fig. 6e). These age populations on the KDE plot also display four main peaks at approximately 435 Ma, 782-988 Ma, 1829 Ma, and 2480 Ma (Fig. 6f).

4.3 Analysis of Jurassic conglomerate clast lithologies

The field provenance analysis of the Lower Jurassic conglomerate

(Shalitashi Formation) reveals significant variations in composition across different sections. In the Kangsu and Wulagen sections, located in the northernmost region of the West Kunlun Range, clasts are composed predominantly of green sandstones (80-51%) and low-grade metamorphic rocks like schist (0-46%), with minor occurrences of light-colored siliceous rock (14-3%) and granitoid (6-0%). In the northwestern sector of the Pamir, a variegated sandstone (22-46%) and a recycled siliceous rock (29-46%) predominantly constitute major clasts in the Oytag and Gaizi sections, respectively (Fig. 3b and 3c). Additionally, minor limestone (11-2%) and diverse igneous rocks (38-6%), including granitoids, rhyolite, and basalts occur characteristically in the same stratigraphic horizon. In the Kyzyltau section (Fig. 3d), the clasts of the Jurassic conglomerate are dominated by green-colored sandstone (28%) and granites (50%) with subordinate schist (13%) and siliceous rock (9%). To the south of Kyzyltau, the Tamu and Qimugen sections present a provenance source dominated by sedimentary rocks. Clasts of limestone (Fig. 3e) and green sandstone account for 85% and 61% in the neighboring sections, respectively. The proportion of reddish sandstone in the Qimugen section (33%) surpasses that in the Tamu section (15%). The Kusilafu section, located to the north of the Kandilik region, exhibits similar clast lithologies in the conglomerate to the Qimugen section, with a predominance of green sandstone (34%) and recycled siliceous rock (45%), along with minor occurrences of reddish sandstone (16%). Detailed clast lithologies and counting results are presented in the Table S4.

4.4 Whole-rock major and trace elements of basalts

406 The chemical compositions of the basalt samples from the Kandilik section
407 are provided in Table S5. Except for one sample (AYBL11D), the majority of our
408 samples displays similar geochemical compositions, characterized by low SiO_2
409 (45.7-51.0 wt.%) and MgO (4.78-7.18 wt.%) contents, and Mg#s ranging
410 between 45 and 52. These samples possess high TiO_2 (2.42-3.34 wt.%) and
411 total alkali (Na_2O+ K_2O = 5.17-6.35 wt.%) contents, exhibit moderate Al_2O_3
412 contents ranging from 11.1 to 14.4 wt.% and total Fe_2O_3 ranging from 12.6 to
413 13.7 wt.%. In comparison, the sample AYBL11D displays relatively high
414 contents of SiO_2 (55.5 wt.%) and TiO_2 (4.76 wt.%) with a low total alkali content
415 (4.80 wt.%). All basalt samples fall within the alkaline series field as depicted in
416 the total alkali-silica diagram (Fig. 7a). However, it is worth noting that all
417 analyzed samples exhibit varying Loss-on-Ignition (LOI = 1.51-9.81 wt.%)
418 values, attributed to weathering and alteration effects, with the presence of
419 chlorite and calcite (Fig. 3m). Hence, it is crucial to assess the alteration effects
420 on the chemical compositions of the analyzed samples. The high-field-strength
421 elements (HFSE, such as Nb, Ta, Ti, and Hf) and rare earth elements (REE)
422 are typically immobile during alteration. This is supported by the consistent
423 elemental variations against the most immobile element Zr, as shown in the Fig.
424 S1. Additionally, Cr and Ni in these samples (except AYBL11D) also
425 demonstrate strong correlations with Zr, suggesting that these elements were
426 essentially immobile during alteration. Based on the Nb/Y vs. Zr/TiO_2 diagram
427 proposed by Winchester and Floyd (1977), all samples plot in the alkaline series
428 (Fig. 7b). Therefore, we posit that these rocks are best classified as alkaline
429 basalt.

430 All analyzed samples display consistent chondrite-normalized rare earth

element patterns (Fig. 7c), characterized by an enrichment of LREE relative to HREE, with $(La/Yb)_N$ ratios ranging from 6.24 to 7.96. Moreover, their REE patterns exhibit slight negative Eu anomalies (δEu = 0.7-1.0). The primitive mantle-normalized multi-element diagram illustrates that the analyzed samples are characterized by the enrichment of highly incompatible trace elements relative to low incompatible elements (Fig. 7d). The samples present significant depletion of Sr and slight enrichment in Zr and Hf. No negative Zr-Hf-Ti anomalies are observed in any of the analyzed basalts.

5 Identification and age constraints for the Lower Jurassic strata

Identified Jurassic strata are largely exposed in the eastern edge of the West Kunlun Mountains and on the southern side along the Talas-Fergana Fault (Fig. 1c). The Jurassic sequences are comprised of coal-bearing siliciclastic rocks with variable thicknesses (Wu et al., 2021). Jurassic volcanic strata have not been previously identified in the West Kunlun Mountains, although a Jurassic tuffaceous succession and Upper Triassic - Lower Jurassic volcanic rocks crop out in the Hindu Kush along the western edge of the Pamir (Brookfield and Hashmat, 2001). Our study has focused on a package of thick clastic rocks intercalated with basaltic lavas, are exposed in the southernmost part of the Jurassic Kyzyltau syncline (Fig. 2). This stratigraphic package was previously considered to be of Mesoproterozoic or Neoproterozoic age due to the lack of fossil records and the presence of low-degree metamorphism (Ma et al., 1991). Lithologically, the monotonous clastic member is composed primarily of gray-black slate and fine - grained sandstone to siltstone, rich in iron and carbonaceous components (Ma et al., 1991). The overlying basalts

vary significantly in their thickness and lithological makeup, composed primarily of basaltic volcanic breccia, amygdaloidal, and massive layers (Fig.3j and 3k).

Our new results of zircon U-Pb dating of basalts and sandstones suggest that this rock assemblage is not Precambrian in age, given the widespread appearance of Phanerozoic ages. We suggest that the weighted mean $^{206}Pb/^{238}U$ age (~178 Ma) of the youngest group of zircons separated from the basalt sample could define the eruptive age of this magmatic episode based on the following lines of evidence. First, these zircons exhibit similar morphological and CL imaging characteristics (Fig. 4), with the majority of the analyzed grains displaying Th/U ratios indicating their igneous origin (Fig. 5d). Secondly, the results of our in-situ trace elemental composition of the zircons (Table S3) indicate that the chondrite-normalized rare earth elements consistently exhibit left-sloping pattern with positive anomalies in Ce and Sm, and negative anomalies in Eu, similar to those of typical igneous zircons (Fig. 5c; Hoskin and Schaltegger, 2003). Thirdly, according to the Y vs. Yb/Sm plot proposed by Belousova et al. (2002), these Jurassic zircons are consistent with the basic or ultrabasic igneous origin (Fig. 5e). Thus, we posit that the crystallization age of the basalt is Toarcian.

To refine the depositional age of the clastic member of the stratigraphy, we have compared the detrital zircon results from the feldspar lithic sandstones with those from the Lower and Middle Jurassic strata, exposed in the Kyzyltau region. The sandstone collected from the Kangsu Formation displayed similar texture and composition to the rocks from the Kandilik region, both composed of immature and poorly sorted quartz and lithic fragments (Fig. 3n and 3o). The age patterns of detrital zircons display remarkably similar populations with Early

Silurian (~440 Ma) and Tonian (~800-950 Ma) dominated peaks, indicating that sediments of the two investigated areas shared a common exhumed provenance. The Lower and Middle Jurassic sedimentary rocks were previously suggested to have been deposited within structural half grabens and mostly sourced from the West Kunlun Mountains (Chen et al., 2018). This interpretation is consistent with our findings. Furthermore, we infer that this stratigraphic package resembles a turbidite sequence, exhibiting relatively proximal, deep-water depositional features.

Accordingly, we propose reassigning this thick package of clastic rocks to the Early - Middle Jurassic age. Hereon, we demonstrate the structural compatibility of this new stratigraphic scheme. The Lower - Middle Jurassic strata of the Yarkant Formation in the studied region comprise a lacustrine association rich in coal beds, and it delineated structurally by a mylonite zone to its west (Fig. 2b). The redefined sequences are rich in carbonaceous components and are closely bounded by Jurassic coal-bearing strata along several reverse faults. These two units successfully extend into the NW-SE-striking Jurassic graben, which surprisingly narrows rapidly towards the south without any obvious facies transition (Fig. 1c). The basin-ward dipping of the strata constituted the western limb of the Jurassic syncline, which has a comparable thickness that may extend into the southern area of the Kyzyltau syncline (Fig. 2).

6 Discussion

6.1 Generation and geological setting of the Early Jurassic volcanism

The basalt samples are characterized by varying SiO_2 (45.7-55.5 wt.%)

and low Mg# values (45-52), suggesting that they were not derived from the primary magmas, and that they likely experienced crustal assimilation and fractional crystallization (AFC) processes. Generally, mantle - derived magmas suffer various degrees of crust contamination en-route from magma chambers to the surface (Aitcheson and Forrest, 1994). The presence of inherited Paleozoic and Neoproterozoic zircons in these basalts suggests the potential interactions between the ascending magmas and the country rocks (Fig. 5a). However, these basaltic rocks exhibit no negative anomalies of Nb, Ta, and Ti, which are typically depleted in the crust (Fig. 7d). They exhibit low La/Nb ratios (0.53 - 1.15) and mostly have high Nb/U ratios (37 - 45), similar to the range of oceanic lavas (La/Nb <1.2 and Nb/U >39; Krienitz et al., 2006). Additionally, all basalt samples exhibit low Th/Nb ratios (0.09-0.15), plotting along the MORB−OIB array of oceanic basalts within the Th/Yb-Nb/Yb diagram (Fig. 7e; Pearce, 2008). These signatures, with little indication of crustal components, suggest that these basalts experienced negligible contamination during their journey to the surface. They are characterized by extremely low concentrations of Ni (27.4–61.2 ppm) and Cr (25.4–108 ppm). They also exhibit slightly negative anomalies of Eu and Sr on the whole-rock normalized REE patterns and spider diagram (Fig. 7c and 7d). These features could be caused by varying degrees of fractional crystallization processes involving olivine, clinopyroxene, and plagioclase.

The Early Jurassic episode of volcanism in the West Kunlun Mountains temporally followed the Cimmerian Orogeny. Regionally, the eruption of basalts at 178 Ma was slightly later than the peak metamorphism of high-pressure granulite facies that has been proposed to have occurred between 200 and 185

Ma (Qu et al., 2021). Collisional orogeny commonly transitions from syn-collisional metamorphism to post-collisional unroofing (Dilek and Altunkaynak, 2007, 2010; Zheng et al., 2019). The unroofing phase could generate geochemically varying granitoids with extrusion of mafic magma (Harris et al., 1986; Zhou et al., 2021). However, distinguishing post-collisional from syn-collisional magmatism may present challenges, because the post-collisional mafic rocks could inherit whole-rock geochemical fingerprints from the preceding subducted materials (Zhao et al., 2013). Conversely, intraplate magmas are typically dominated by low-degree partial melting and silica-unsaturated alkaline magmas, which is distinct from syn- and post-collisional igneous rocks (Dilek and Altunkaynak, 2010; Xu et al., 2020).

The Jurassic alkali basalts exhibit enrichment of LREE and HSFEs without obvious crustal signatures (e.g., Nb-Ta depletion; Fig. 7c-d), different from the syn- and post-collisional magmas in the West Kunlun Mountains (Liao et al., 2012; Chen et al., 2021). Their compositions resemble those of intraplate OIBs and could have been generated by low-degree partial melting (~5%) of a garnet lherzolite mantle source (Fig. 7e-f). All tectonic discrimination plots using immobile trace elements indicate that the Jurassic basalts formed within an intraplate setting (Fig. 8).

The generation of these magmas can be attributed to one of two mechanisms. The first explanation is that the North Kunlun region experienced rapid orogenic collapse after Late Triassic collisional orogeny, during which intra-plate collapse-related volcanism generate the observed basalt flows. We do not find this hypothesis plausible given the implied rapid transition from peak collisional orogeny, including ca. 185 Ma prograde metamorphism, to collapse

and volcanism recorded at ca. 175 Ma (Wu et al., 2021). Many arc-continent or continent-continent collisional orogens, evolving from peak orogenic metamorphism, to orogenic collapse, to intraplate stage, collectively persist for tens of millions of years (Dewey, 2005; Weller et al., 2021). Conversely, a broad plate-boundary extensional process may have impacted this orogenic belt and its hinterland region in the Early Jurassic. Support for this model includes the expansive extensional rifts developed across the marginal and interior Eurasia during the Early-Middle Jurassic (e.g., Amu–Dar'ya, Afghan–Tajik and Fergana basins; Otto, 1997; Golonka, 2004).

6.2 Jurassic basin formation and implications for sedimentary provenance

The closure of the Paleo-Tethyan Ocean led to collision of the Cimmerian terranes with Eurasia that caused the development of a regional unconformity across the central Asia during the Triassic to Early Jurassic (Gaetani et al., 1993; Schwab et al., 2004; Fürsich et al., 2017). In the studied area, the deformed Upper Paleozoic strata are unconformably overlain by a Lower Jurassic conglomerate (Fig. 9).

The Kyzyltau basin preserves the most comprehensive record of the formation and evolution of a post-Cimmerian rift, spanning from its initiation in the Early Jurassic to its inversion in the Late Jurassic (Wu et al., 2021). The basement of this basin varies along its lateral extent, indicating its strong tectonic reworking prior to Jurassic deposition. It comprises four subdivisions from the north to the southeast: (1) an Early Devonian metasedimentary rock terrane in the Kashgar depression (1-4 in Fig. 9), (2) the Carboniferous island-

arc crust and Permian back-arc basin successions in the NW segment of the West Kunlun (5-6 in Fig. 9), (3) an Upper Carboniferous to Middle Permian platform successions in the middle segment (7-11 in Fig. 9), and (4) an Upper Permian clastic formation in the southern part (12-17 in Fig. 9).

The massive conglomerate of the Shalitashi Formation indicates rapid infilling of the Jurassic basin during its initial opening stage. Analysis of conglomerate clast lithologies from different sites suggests significant compositional variations, consistent with the presence of local basement rocks (Fig. 9). For example, the arenaceous gravels in the Kashgar depression are primarily derived from the underlying Devonian (Wulagen) uplift. The gravels from the Oytag and Gaizi contain abundant igneous and siliceous rock fragments, which may have been sourced from the local arc and back-arc basin lithologies. Contrastively, gravels from the Tamu are composed predominately of limestones, implying their origin from the underlying Carboniferous marine strata. The Qimugen and Kusilafu share a similar arenaceous source region, located within the Devonian and Permian strata in the core of the Kashgar-Yecheng syncline (Fig. 2a).

The Lower Jurassic strata rapidly transition from alluvial fan deposits into fluvial sedimentary environment. During the Middle Jurassic, a sequence of stacked coal-bearing sandstones was deposited (Fig. 9). Extensional faulting across the half-grabens further deepened the basin and facilitated the deposition of a turbidite sequence in the Yangye Formation (Wu et al., 2021). Provenance analysis based on detrital zircons suggests that the source region for these sandstones was dominated by Late Ordovician-Early Silurian (~ 446 - 435 Ma) and Neoproterozoic (~ 980 - 780 Ma) igneous rocks, with minor

606 Neoarchean-Paleoproterozoic and Mesoproterozoic ages (Fig. 6). Early
607 Paleozoic (~ 480 - 440 Ma) granitoids, with a peak intrusive at ~ 440 Ma (Fig.
608 1c; Tao et al., 2024), are exposed extensively in the South Kunlun terrane.
609 However, the South Kunlun terrane is unlikely to be the source for these
610 Jurassic depositions because the South Kunlun region contains extensive
611 Triassic (~ 240 - 210 Ma) granitoids, intruded into the early Paleozoic rock units
612 (Fig. 1c; Chen et al., 2021). Yet, Triassic detrital zircons are absent in the Lower
613 - Middle Jurassic strata (Fig. 6). Therefore, we instead suggest that the potential
614 source area was most likely the North Kunlun terrane, which consists mainly of
615 Paleozoic strata and Precambrian metamorphic basements. A provenance
616 study has revealed that the age patterns of detrital zircons from the Ordovician
617 - Devonian strata contain main age peaks at 430 - 445 Ma, 930 - 800 Ma, and
618 790 - 760 Ma, with subordinate Neoarchean to Mesoproterozoic ages (Yan,
619 2022). Our results are consistent with this detrital zircon age information from
620 the Lower Paleozoic sedimentary rocks and with the paleocurrent results of
621 previous studies (Wu et al., 2021).

622 A Late Jurassic contractional event affected this region, as evidenced by
623 the intense deformation and metamorphism displayed by various formations
624 and rock units (Robinson et al., 2007; Groppo et al., 2019), and by the uplift
625 and inversion of the earlier basin (Yang et al., 2017). The Middle Jurassic
626 shallow marine sequences in South Qiangtang and SE Pamir were uniformly
627 eroded during this time period (Ma et al., 2023). The Upper Jurassic strata are
628 either entirely absent or locally replaced by conglomerate deposits (Fig. 10). In
629 the Tarim Basin, the Upper Jurassic strata are dominated by brownish reddish
630 conglomerate. Previous studies have suggested that these redbeds may

631 indicate a regional increase in aridity resulting from the uplift of the surrounding
632 mountain belts (Hendrix, 2000). The Late Jurassic uplift event has also been
633 supported by numerous thermochronologic ages (170-155 Ma) within the West
634 Kunlun Mountains and Pamir (Fig.1c; Yang et al., 2017). The uplift event also
635 resulted in significant changes in basin and range patterns, and influenced the
636 potential provenance of sediments. The emergence of juvenile detrital zircons
637 in these Upper Jurassic and Lower Cretaceous deposits indicates the
638 exhumation and erosion of a late Paleozoic to Mesozoic arc system (Fig. 10).
639 The Triassic batholiths were thrust onto the southwestern margin of the Tarim
640 Basin creating an elevated topography, which in turn provided abundant clastic
641 material into the Cretaceous depocenters in the region.

642 In summary, the Early Jurassic basin developed on a post-orogenic
643 unconformity. Provenance analysis indicates that the Early to Middle Jurassic
644 sediments were deposited in a half-graben setting and sourced from the
645 proximal basement of the North Kunlun terrane. This basin was subsequently
646 inverted during the Late Jurassic, driven by the contraction and uplift of the
647 surrounding mountains.

648

649 **6.3 Switching extensional and contractional tectonics related to the**
650 **subduction of Neo-Tethys**

651 The Mesozoic era records the transition from the closure of the Paleo-
652 Tethys Ocean to the initiation of subduction within Neo-Tethys (Wan et al., 2019).
653 These processes are influenced by complex plate tectonic conditions, as the
654 evolution of the Paleo- and Neo-Tethys Oceans varies significantly in their time-
655 space patterns. The two Tethyan seaways diverge into several branches

656 extending from Iran to Pamir, then eastward into the Tibetan Plateau (Fig. 1a).
657 Deciphering the history of the Pamir Tethyan segment, therefore, improves our
658 knowledge of the geodynamic evolution of the entire Tethyan realm.

659 Two major tectonic events profoundly affected the sedimentary patterns of
660 the Mesozoic successions in this region. Episodic collisions along the southern
661 Asian margin in the Late Triassic and then in the Late Jurassic resulted in major
662 deformation (Jolivet, 2017). The regional magmatic history and the results of
663 the provenance studies of the Jurassic basin necessitate a geodynamic
664 scenario to explain the mechanism of an extensional tectonic event between
665 two major contractional events. Although a flat subduction model has recently
666 been proposed to explain the regional Cretaceous magmatism in the Pamir, the
667 mode of Jurassic tectonic processes remains poorly constrained (Chapman et
668 al., 2018). As discussed above, the history of the Neo-Tethyan subduction
669 events significantly varies spatially. The initiation of subduction along the
670 Tibetan margin occurred during the Middle Triassic, leading to volcanic
671 activities in the southern Lhasa (Wang et al., 2016; Xie et al., 2021), whereas
672 the subduction in the Iran sector in the same orogenic belt farther west initiated
673 later in the Early Jurassic (Wan et al., 2023). The extensive Early-Middle arc
674 Jurassic magmatism along both continental margins indicates a synchronous
675 flare-up of continental arcs (Fig. 11a and 11c). The bimodal volcanism (195-174
676 Ma) in the Gangdese arc was associated with the subsequent opening of a
677 back-arc basin (174-156 Ma) (Fig. 11c; Kapp and DeCelles, 2019). The
678 magmatic arc of the Sanandaj–Sirjan belt (180-140 Ma) in SW Iran was
679 facilitated by a simultaneous progressive back-arc rift (Fig. 11a; Hassanzadeh
680 and Wernicke, 2016; Azizi and Stern, 2019).

By comparison, compiled magmatic detrital zircons in the Pamir segment reveal that Early-Middle Jurassic magmatism was almost absent there (Fig. 11b; Chapman et al., 2018). Available geochronological data indicate that Jurassic igneous rocks surrounding the Pamir are also limited (Fig. 6), with only basalts exposed in the North Kunlun (Kandilik) and Tianshuihai regions (Jian et al., 2019) and bimodal volcanic rock suites found in the east of Karakoram (Zhou et al., 2019). Geochemical studies reveal that these coeval basaltic lavas (178-174 Ma) exhibit distinct features in their major and trace element compositions (Fig. 7). Magmas of the basaltic lavas in the North Kunlun were dominated by within-plate basalts that shared similar compositions with typical OIB (Fig. 7 and 8). In contrast, basalts in the Tianshuihai to the south were dominated by back-arc MORBs (Fig. 8a-c), characterized by distinct Nb-Ta depletions (Fig. 7d). The scarcity of zircon-rich felsic magmas in this region evidently differs from the conditions in the western and eastern segments of the Eurasian Tethyan margins where arc magmatism developed upon continental basement. To date, the exact timing of the onset of subduction-related magmatism in the Pamir Tethyan margin remains unclear. The geochronological dataset for the Karakoram arc and the Kohistan Ladakh arc indicates that magmatic activity may have occurred as early as the Late Jurassic (Fig. 11b; Jagoutz et al., 2018; Saktura et al., 2023).

While the spatial continuity of the Tethyan suture zones from Iran into Tibet remains enigmatic, we propose that the regional Early to Middle Jurassic extension expressed across the southern Eurasian continental margin was a consequence of retreating subduction of the Neo-Tethyan Ocean floor. First, the transition from Cimmerian orogenic build-up (200-185 Ma) to large-scale

706 continental extension (178-174 Ma) suggests the involvement of additional
707 external extensional stresses, different from the classic cases of continent -
708 continent collision (Weller et al., 2021). Secondly, the 195 Ma bimodal volcanic
709 rocks in Karakoram and the 174 Ma MORB-like basalts in Tianshuihai have
710 been suggested as associated with the initial opening of a back-arc basin,
711 based on their geochemical signatures of crustal material metasomatism (Jian
712 et al., 2019; Zhou et al., 2019). The magmatism in Pamir and Karakoram was
713 quite similar to the extensional episodes that occurred in the southern margin
714 of the Lhasa block, caused by accelerated slab rollback (Kapp and DeCelles,
715 2019). Thirdly, deposition of shallow marine carbonates was prevalent in the
716 Pamir and Karakoram during the Middle Jurassic (Fig. 10), indicating an
717 expansive extensional continental platform facing the ocean (Yang et al., 2017).
718 These scenarios are analogous to the active margin of the western Pacific rim,
719 which is characterized by a broad marginal sea with an outboard trench -
720 subduction chain (Fig. 1a). Additionally, the Middle Jurassic extension occurred
721 across the broad hinterlands of central Asia, which cannot be easily explained
722 by the collapse of the Paleo-Tethyan orogenic belt (Otto, 1997).

723 During the Late Jurassic, this marginal extensional basin started to invert,
724 with extensive contractional deformation of the Lower-Middle Jurassic
725 carbonate strata and the development of a major angular unconformity (Fig. 10;
726 Gaetani et al., 1993; Robinson, 2015). Available basement thermochronological
727 data show widespread exhumation across the West Kunlun Mountains (Fig. 1c),
728 as well as the reactivation of the Paleo-Tethyan sutures within the Pamir
729 terranes (Schwab et al., 2004). The exhumation of the Triassic plutons in the
730 South Kunlun Mountain led to the transport of debris material from the

magmatic arc into the Tarim basin through braided fluvial network systems (Fig. 11b). This broad uplift event has been interpreted as retro-arc deformation and shortening related to the advancing subduction of the Neo-Tethyan Ocean (Robinson, 2015).

The subduction style along the broader strike-length of the Tethyan orogen varied from the west to the east in the Late Jurassic - Early Cretaceous. Similar to the West Kunlun Mountains, the Lhasa block to the east experienced basin inversion and contractional deformation starting by ca. 155 Ma and throughout the Early Cretaceous (e.g., Murphy et al., 1997; Ding and Lai, 2003; Kapp and DeCelles, 2019). Geological mapping has documented significant shortening strain (~ 60%) across Lhasa at this time (Murphy et al., 1997). Although the cause of this event has been debated, the magmatic lull since the earliest Cretaceous and subsequent flare-up in the Mid-Cretaceous in both regions imply that they shared a similar geodynamic setting (Fig. 11; Chapman et al., 2018). A major tectonic event involving intense folding and thrusting occurred also around 166 Ma in the South Qiangtang Block, resulting in two phases of southward retreat of the remnant seaway of the Meso-Tethys (Ma et al., 2017a, 2018). A previous study proposed that the development of Jurassic basin inversion in the Tibetan Plateau may be related to the accretion of microcontinents onto the South Qiangtang margin, driven by the northward subduction of the Bangong-Nujiang Ocean (Ma et al., 2023). Conversely, the Iranian segment to the west experienced continuous extension at the same time (Hunziker et al., 2015; Lechmann et al., 2018; Maghdour-Mashhour et al., 2021). These along-strike variations likely reflect broad geodynamic changes to, or initial conditions of, the Tethyan Ocean system that warrant future investigations.

For example, variable plate convergence rates related to global tectonic configurations or the oceanic-plate age variations could result in unique tectonic events along the strike-length of the entire Tethyan orogen. Alternatively, the closure of the Bangong-Nujiang Ocean, another branch of the Tethyan system between the Lhasa and Qiangtang blocks, might have also played a significant role in along-strike variations within the Tethyan orogenic belt (Fig. 11; Yang et al., 2017; Kapp and DeCelles, 2019).

7 Conclusion

This study has concentrated on the stratigraphy and provenance of Jurassic strata in the West Kunlun Mountains to better understand the Mesozoic geological evolution of the Eurasian margin within the framework of the Tethyan geodynamics. Our investigations of the Jurassic sedimentary successions, combined with new geochronological and geochemical data from coeval basaltic lava intercalations, led to the following conclusions:

(1) A newly identified, thick sedimentary package with basaltic lava interlayers in the southern end of the Kyzyltau basin bears similarities to the Lower and Middle Jurassic sequences in their clastic compositions and structures. Zircon U-Pb dating results from basaltic lavas suggest an Early Jurassic age (~ 178 Ma) for this stratigraphic member, in contrast to a Precambrian age previously reported. This is a significant change that strongly affects the current tectonic interpretations and models.

(2) Our new geochemical data from the Early Jurassic basaltic extrusive rocks show that magmas of these basalts had typical OIB affinities, and that they lacked crustal contamination. Thus, the related magmatism likely occurred

781 in an intraplate rifting setting and was facilitated by extensional fault systems,
782 which significantly reduced the residence time of the ascending magmas in the
783 crust avoiding contamination.

784 (3) Provenance analysis, integrating conglomerate clast lithologies with
785 detrital zircons, indicates a significant source contribution from local basements
786 (North Kunlun) for the Early to Middle Jurassic rift basins. In comparison, the
787 Late Jurassic contractional event caused an uplift of the surrounding mountains
788 in the South Kunlun and Pamir, significantly influencing the basin
789 tectonostratigraphy and source- to -sink system.

790 (4) The Jurassic switching extensional and contractional tectonics in the
791 West Kunlun Mountains and a wider region across the southern Eurasian
792 margin are related to changes in the subduction style of the Neo-Tethyan Ocean
793 floor, transitioning from retreating in Early - Middle Jurassic to advancing in Late
794 Jurassic - Early Cretaceous. Additionally, the Pamir and West Kunlun regions,
795 as the central junction of the Tethys orogenic belt, share a comparable
796 Mesozoic history of extensional and contractional structures with that of the
797 Tibetan Plateau.

798

799 **Declaration of Competing Interest**

800 The authors declare that they have no known competing financial interests
801 or personal relationships that could have appeared to influence the work
802 reported in this paper.

803

Acknowledgement

We gratefully acknowledged the constructive and insightful reviews by two anonymous reviewers, and the effective editorial handling of Federico Rossetti and Yang Chu. This work was supported by the National Natural Science Foundation of China (Grants No. U22B6002 and 42302231). H.-X. Wu received the funding of Postdoctoral Science Foundation (2023M742979 and 2024T170768).

Author Contributions

Hong-Xiang Wu: Conceptualization, Formal Analysis, Investigation, Methodology, Visualization, Writing – original draft, Writing – review & editing, Funding acquisition; *Han-Lin Chen:* Funding acquisition, Investigation, Project administration; *Andrew V. Zuza: Writing – review & editing; Yildirim Dilek: Writing – review & editing; Du-Wei Qiu:* Investigation, Formal Analysis; *Qi-Ye Lu:* Investigation, Formal Analysis; *Feng-Qi Zhang:* Investigation, Formal Analysis; *Xiao-Gan Cheng:* Investigation*; Xiu-Bin Lin:* Investigation.

Data availability

The data used in this study are available in the references and Supplementary Material, including five tables and one figure.

825 **References**

826 Aldanmaz, E., Pearce, J. A., Thirlwall, M. F., and Mitchell, J. G.: Petrogenetic
827 evolution of late Cenozoic, post-collision volcanism in western Anatolia,
828 Turkey, Journal of Volcanology and Geothermal Research, 102, 67-95,
829 https://doi.org/10.1016/S0377-0273(00)00182-7, 2000.
830 Andersen, T.: Correction of common lead in U–Pb analyses that do not report
831 204Pb, Chemical Geology, 192, 59-79, https://doi.org/10.1016/S0009-
832 2541(02)00195-X, 2002.
833 Angiolini, L., Zanchi, A., Zanchetta, S., Nicora, A., Vuolo, I., Berra, F.,
834 Henderson, C., Malaspina, N., Rettori, R., Vachard, D., and Vezzoli, G.:
835 From rift to drift in South Pamir (Tajikistan): Permian evolution of a
836 Cimmerian terrane, Journal of Asian Earth Sciences, 102, 146-169,
837 https://doi.org/10.1016/j.jseaes.2014.08.001, 2015.
838 Angiolini, L., Zanchi, A., Zanchetta, S., Nicora, A., and Vezzoli, G.: The
839 Cimmerian geopuzzle: new data from South Pamir, Terra Nova, 25, 352-
840 360, https://doi.org/10.1111/ter.12042, 2013.
841 Aitcheson, S. J. and Forrest, A. H.: Quantification of Crustal Contamination in
842 Open Magmatic Systems, Journal of Petrology, 35, 461-488,
843 10.1093/petrology/35.2.461, 1994.
844 Azizi, H. and Stern, R. J.: Jurassic igneous rocks of the central Sanandaj–Sirjan
845 zone (Iran) mark a propagating continental rift, not a magmatic arc, Terra
846 Nova, 31, 415-423, https://doi.org/10.1111/ter.12404, 2019.
847 Belousova, E., Griffin, W., O'Reilly, S. Y., and Fisher, N.: Igneous zircon: trace
848 element composition as an indicator of source rock type, Contributions to
849 Mineralogy and Petrology, 143, 602-622, 10.1007/s00410-002-0364-7,

2002.

Brookfield, M. E. and Hashmat, A.: The geology and petroleum potential of the North Afghan platform and adjacent areas (northern Afghanistan, with parts of southern Turkmenistan, Uzbekistan and Tajikistan), Earth-Science Reviews, 55, 41-71, https://doi.org/10.1016/S0012-8252(01)00036-8, 2001.

Burtman, V. S. and Molnar, P.: Geological and Geophysical Evidence for Deep Subduction of Continental Crust Beneath the Pamir, in: Geological and Geophysical Evidence for Deep Subduction of Continental Crust Beneath the Pamir, Geological Society of America, 0, 10.1130/SPE281-p1, 1993.

Cabanis, B. and Lecolle, M.: The La/10-Y/15-Nb/8 diagram: a tool for discriminating volcanic series and evidencing continental crust magmatic mixtures and/or contamination, Comptes Rendus - Academie des Sciences, Serie II, 309, 2023-2029, 1989.

Cao, K., Wang, G.-C., Bernet, M., van der Beek, P., and Zhang, K.-X.: Exhumation history of the West Kunlun Mountains, northwestern Tibet: Evidence for a long-lived, rejuvenated orogen, Earth and Planetary Science Letters, 432, 391-403, https://doi.org/10.1016/j.epsl.2015.10.033, 2015.

Cao, W., Zahirovic, S., Flament, N., Williams, S., Golonka, J., and Müller, R. D.: Improving global paleogeography since the late Paleozoic using paleobiology, Biogeosciences, 14, 5425-5439, 10.5194/bg-14-5425-2017, 2017.

Chapman, J. B., Scoggin, S. H., Kapp, P., Carrapa, B., Ducea, M. N., Worthington, J., Oimahmadov, I., and Gadoev, M.: Mesozoic to Cenozoic

875 magmatic history of the Pamir, Earth and Planetary Science Letters, 482,
876 181-192, https://doi.org/10.1016/j.epsl.2017.10.041, 2018.
877 Chen, S., Chen, H., Zhu, K., and Tao, Y.: Petrogenesis of the Middle–Late
878 Triassic S- and I-type granitoids in the eastern Pamir and implications for
879 the Tanymas–Jinshajiang Paleo-Tethys Ocean, International Journal of
880 Earth Sciences, 110, 1213-1232, 10.1007/s00531-021-02013-z, 2021.
881 Chen, Y., Wu, H., Zhang, L., Cheng, X., Chen, C., Zhang, Y., Ren, P., Zhang, F.,
882 and Chen, H.: Characteristics of the Late Triassic paleo-structure in the
883 mountain front region of western Kunlun and its control of Jurassic-
884 Cretaceous deposition, Chinese Journal of Geology, 53, 1405-1418, 2018
885 (in Chinese with English abstract).
886 Corfu, F., Hanchar, J. M., Hoskin, P. W. O., and Kinny, P.: Atlas of Zircon
887 Textures, Reviews in Mineralogy and Geochemistry, 53, 469-500,
888 10.2113/0530469, 2003.
889 Cowgill, E.: Cenozoic right-slip faulting along the eastern margin of the Pamir
890 salient, northwestern China, GSA Bulletin, 122, 145-161,
891 10.1130/b26520.1, 2010.
892 Dewey, J. F.: Orogeny can be very short, Proceedings of the National Academy
893 of Sciences, 102, 15286-15293, doi:10.1073/pnas.0505516102, 2005.
894 Dilek, Y. and Altunkaynak, Ş.: Cenozoic Crustal Evolution and Mantle Dynamics
895 of Post-Collisional Magmatism in Western Anatolia, International Geology
896 Review, 49, 431-453, 10.2747/0020-6814.49.5.431, 2007.
897 Dilek, Y. and Altunkaynak, Ş.: Geochemistry of Neogene–Quaternary alkaline
898 volcanism in western Anatolia, Turkey, and implications for the Aegean
899 mantle, International Geology Review, 52, 631-655,

10.1080/00206810903495020, 2010.

Dilek, Y. and Furnes, H.: Tethyan ophiolites and Tethyan seaways, Journal of the Geological Society, 176, 899-912, doi:10.1144/jgs2019-129, 2019.

Dilek, Y. and Moores, E. M.: Regional tectonics of the eastern Mediterranean ophiolites. In: J. Malpas, E. M. Moores, A. Panayiotou, and C. Xenophontos (Eds), Ophiolites. Oceanic Crustal Analogues, Proceedings of the Symposium “Troodos 1987’, The Geological Survey Department, Nicosia, Cyprus, 295–309, 1990.

Ding, L. and Lai, Q.: New geological evidence of crustal thickening in the Gangdese block prior to the Indo-Asian collision, Chinese Science Bulletin, 48, 1604-1610, 10.1007/BF03183969, 2003.

Dong, Y., He, D., Sun, S., Liu, X., Zhou, X., Zhang, F., Yang, Z., Cheng, B., Zhao, G., and Li, J.: Subduction and accretionary tectonics of the East Kunlun orogen, western segment of the Central China Orogenic System, Earth-Science Reviews, 186, 231-261, https://doi.org/10.1016/j.earscirev.2017.12.006, 2018.

Faisal, S., Larson, K. P., Cottle, J. M., and Lamming, J.: Building the Hindu Kush: monazite records of terrane accretion, plutonism and the evolution of the Himalaya–Karakoram–Tibet orogen, Terra Nova, 26, 395-401, https://doi.org/10.1111/ter.12112, 2014.

Fürsich, F. T., Brunet, M.-F., Auxiètre, J.-L., and Munsch, H.: Lower–Middle Jurassic facies patterns in the NW Afghan–Tajik Basin of southern Uzbekistan and their geodynamic context, in: Geological Evolution of Central Asian Basins and the Western Tien Shan Range, edited by: Brunet, M. F., McCann, T., and Sobel, E. R., Geological Society of London, 0,

925 10.1144/sp427.9, 2017.
926 Gaetani, M., Jadoul, F., Erba, E., and Garzanti, E.: Jurassic and Cretaceous
927 orogenic events in the North Karakoram: age constraints from sedimentary
928 rocks, Geological Society, London, Special Publications, 74, 39-52,
929 doi:10.1144/GSL.SP.1993.074.01.04, 1993.
930 Golonka, J.: Plate tectonic evolution of the southern margin of Eurasia in the
931 Mesozoic and Cenozoic, Tectonophysics, 381, 235-273,
932 https://doi.org/10.1016/j.tecto.2002.06.004, 2004.
933 Groppo, C., Rolfo, F., McClelland, W. C., and Coble, M. A.: Pre-Cenozoic
934 evolution of the Aghil Range (western Tibetan Plateau): A missing piece of
935 the Tibet-Pamir-Karakorum geopuzzle, Gondwana Research, 69, 122-143,
936 https://doi.org/10.1016/j.gr.2018.12.006, 2019.
937 Guo, P., Niu, Y., Sun, P., Gong, H., and Wang, X.: Lithosphere thickness
938 controls continental basalt compositions: An illustration using Cenozoic
939 basalts from eastern China, Geology, 48, 128-133, 10.1130/g46710.1,
940 2020.
941 Harris, N. B. W., Pearce, J. A., and Tindle, A. G.: Geochemical characteristics
942 of collision-zone magmatism, Geological Society, London, Special
943 Publications, 19, 67-81, doi:10.1144/GSL.SP.1986.019.01.04, 1986.
944 Hassanzadeh, J. and Wernicke, B. P.: The Neotethyan Sanandaj-Sirjan zone
945 of Iran as an archetype for passive margin-arc transitions, Tectonics, 35,
946 586-621, https://doi.org/10.1002/2015TC003926, 2016.
947 Hendrix, M. S.: Evolution of Mesozoic Sandstone Compositions, Southern
948 Junggar, Northern Tarim, and Western Turpan Basins, Northwest China: A
949 Detrital Record of the Ancestral Tian Shan, Journal of Sedimentary

Research, 70, 520-532, doi:10.1306/2dc40924-0e47-11d7-8643000102c1865d, 2000.

Hendrix, M. S., Graham, S. A., Carroll, A. R., Sobel, E. R., McKnight, C. L., Schulein, B. J., and Wang, Z.: Sedimentary record and climatic implications of recurrent deformation in the Tian Shan: Evidence from Mesozoic strata of the north Tarim, south Junggar, and Turpan basins, northwest China, GSA Bulletin, 104, 53-79, 10.1130/0016-7606(1992)104<0053:Sracio>2.3.Co;2, 1992.

Hoskin, P. W. O. and Schaltegger, U.: The Composition of Zircon and Igneous and Metamorphic Petrogenesis, Reviews in Mineralogy and Geochemistry, 53, 27-62, 10.2113/0530027, 2003.

Hunziker, D., Burg, J.-P., Bouilhol, P., and von Quadt, A.: Jurassic rifting at the Eurasian Tethys margin: Geochemical and geochronological constraints from granitoids of North Makran, southeastern Iran, Tectonics, 34, 571-593, https://doi.org/10.1002/2014TC003768, 2015.

Hou, Z., Duan, L., Lu, Y., Zheng, Y., Zhu, D., Yang, Z., Yang, Z., Wang, B., Pei, Y., Zhao, Z., and McCuaig, T. C.: Lithospheric Architecture of the Lhasa Terrane and Its Control on Ore Deposits in the Himalayan-Tibetan Orogen*, Economic Geology, 110, 1541-1575, 10.2113/econgeo.110.6.1541, 2015.

Jafari, A., Ao, S., Jamei, S., and Ghasemi, H.: Evolution of the Zagros sector of Neo-Tethys: Tectonic and magmatic events that shaped its rifting, seafloor spreading and subduction history, Earth-Science Reviews, 241, 104419, https://doi.org/10.1016/j.earscirev.2023.104419, 2023.

Jagoutz, O., Bouilhol, P., Schaltegger, U., and Müntener, O.: The isotopic evolution of the Kohistan Ladakh arc from subduction initiation to continent

975 arc collision, in: Himalayan Tectonics: A Modern Synthesis, edited by:
976 Treloar, P. J., and Searle, M. P., The Geological Society of London, 0,
977 10.1144/sp483.7, 2019.
978 Jian, K., Gao, F., Du, B., Zhang, Z., Wang, X., and Zhao, D.: Formation age,
979 geochemical characteristics and tectonic setting of the basalts from
980 Longshan Formation in Heweitan area, Karakorum, J Mineral Petrol, 39,
981 42-51, 2019 (in Chinese with English abstract).
982 Jolivet, M.: Mesozoic tectonic and topographic evolution of Central Asia and
983 Tibet: a preliminary synthesis, Geological Society, London, Special
984 Publications, 427, 19-55, doi:10.1144/SP427.2, 2017.
985 Kapp, P. and DeCelles, P. G.: Mesozoic–Cenozoic Geological Evolution of the
986 Himalayan-Tibetan Orogen and Working Tectonic Hypotheses, American
987 Journal of Science, 319, 159-+, 10.2475/03.2019.01, 2019.
988 Kapp, P., DeCelles, P. G., Gehrels, G. E., Heizler, M., and Ding, L.: Geological
989 records of the Lhasa-Qiangtang and Indo-Asian collisions in the Nima area
990 of central Tibet, GSA Bulletin, 119, 917-933, 10.1130/b26033.1, 2007.
991 Kazmin, V. G.: Collision and rifting in the Tethys Ocean: geodynamic implication,
992 Tectonophysics, 196, 371-384, https://doi.org/10.1016/0040-
993 1951(91)90331-L, 1991.
994 Krienitz, M. S., Haase, K. M., Mezger, K., Eckardt, V., and Shaikh-Mashail, M.
995 A.: Magma genesis and crustal contamination of continental intraplate
996 lavas in northwestern Syria, Contributions to Mineralogy and Petrology,
997 151, 698-716, 10.1007/s00410-006-0088-1, 2006.
998 Lechmann, A., Burg, J.-P., Ulmer, P., Mohammadi, A., Guillong, M., and Faridi,
999 M.: From Jurassic rifting to Cretaceous subduction in NW Iranian

1000 Azerbaijan: geochronological and geochemical signals from granitoids,
1001 Contributions to Mineralogy and Petrology, 173, 102, 10.1007/s00410-018-
1002 1532-8, 2018.
1003 Leith, W.: A mid-Mesozoic extension across Central Asia?, Nature, 313, 567-
1004 570, 10.1038/313567a0, 1985.
1005 Li, G., Sandiford, M., Fang, A., Kohn, B., Sandiford, D., Fu, B., Zhang, T., Cao,
1006 Y., and Chen, F.: Multi-stage exhumation history of the West Kunlun orogen
1007 and the amalgamation of the Tibetan Plateau, Earth and Planetary Science
1008 Letters, 528, 115833, https://doi.org/10.1016/j.epsl.2019.115833, 2019.
1009 Li, L., Najman, Y., Dupont-Nivet, G., Parra, M., Roperch, P., Kaya, M., Meijer,
1010 N., O'Sullivan, P., Jepson, G., and Aminov, J.: Mesozoic–Cenozoic
1011 multistage tectonic evolution of the Pamir: Detrital fission-track constraints
1012 from the Tajik Basin, Basin Research, 35, 530-550,
1013 https://doi.org/10.1111/bre.12721, 2023.
1014 Li, S., Zhao, S., Liu, X., Cao, H., Yu, S., Li, X., Somerville, I., Yu, S., and Suo,
1015 Y.: Closure of the Proto-Tethys Ocean and Early Paleozoic amalgamation
1016 of microcontinental blocks in East Asia, Earth-Science Reviews, 186, 37-
1017 75, https://doi.org/10.1016/j.earscirev.2017.01.011, 2018.
1018 Li, Y., Robinson, A. C., Zucali, M., Gadoev, M., Oimuhammadzoda, I., Lapen, T.
1019 J., and Carrapa, B.: Mesozoic Tectonic Evolution in the Kurgovat-Vanch
1020 Complex, NW Pamir, Tectonics, 41, e2021TC007180,
1021 https://doi.org/10.1029/2021TC007180, 2022b.
1022 Liao, S., Jiang, Y., Zhou, Q., Yang, W., Jin, G., and Zhao, P.: Geochemistry and
1023 geodynamic implications of the Triassic bimodal magmatism from Western
1024 Kunlun Orogen, northwest China, International Journal of Earth Sciences,

101, 555-577, 10.1007/s00531-011-0686-7, 2012.

Ma, A., Hu, X., Garzanti, E., Han, Z., and Lai, W.: Sedimentary and tectonic evolution of the southern Qiangtang basin: Implications for the Lhasa-Qiangtang collision timing, Journal of Geophysical Research: Solid Earth, 122, 4790-4813, https://doi.org/10.1002/2017JB014211, 2017a.

Ma, A., Hu, X., Kapp, P., Han, Z., Lai, W., and BouDagher-Fadel, M.: The disappearance of a Late Jurassic remnant sea in the southern Qiangtang Block (Shamuluo Formation, Najiangco area): Implications for the tectonic uplift of central Tibet, Palaeogeography, Palaeoclimatology, Palaeoecology, 506, 30-47, https://doi.org/10.1016/j.palaeo.2018.06.005, 2018.

Ma, S., Wang, Y., and Fang, X.: Basic characteristics of Proterozoic Eonothem as a table cover on northern slope, Xinjiang Geology, 9, 59-71, 1991 (in Chinese with English abstract).

Ma, X., Xu, Z., Meert, J., and Santosh, M.: Early Jurassic intra-oceanic arc system of the Neotethys Ocean: Constraints from andesites in the Gangdese magmatic belt, south Tibet, Island Arc, 26, e12202, https://doi.org/10.1111/iar.12202, 2017b.

Maghdour-Mashhour, R., Hayes, B., Pang, K.-N., Bolhar, R., Tabbakh Shabani, A. A., and Elahi-Janatmakan, F.: Episodic subduction initiation triggered Jurassic magmatism in the Sanandaj–Sirjan zone, Iran, Lithos, 396-397, 106189, https://doi.org/10.1016/j.lithos.2021.106189, 2021.

Mattern, F. and Schneider, W.: Suturing of the Proto- and Paleo-Tethys oceans in the western Kunlun (Xinjiang, China), Journal of Asian Earth Sciences, 18, 637-650, https://doi.org/10.1016/S1367-9120(00)00011-0, 2000.

Meschede, M.: A method of discriminating between different types of mid-ocean

ridge basalts and continental tholeiites with the Nb 1bZr 1bY diagram, Chemical Geology, 56, 207-218, https://doi.org/10.1016/0009-2541(86)90004-5, 1986.

Metcalfe, I.: Gondwana dispersion and Asian accretion: Tectonic and palaeogeographic evolution of eastern Tethys, Journal of Asian Earth Sciences, 66, 1-33, 10.1016/j.jseaes.2012.12.020, 2013.

Metcalfe, I.: Multiple Tethyan ocean basins and orogenic belts in Asia, Gondwana Research, 100, 87-130, https://doi.org/10.1016/j.gr.2021.01.012, 2021.

Middlemost, E. A. K.: Naming materials in the magma/igneous rock system, Earth-Science Reviews, 37, 215-224, https://doi.org/10.1016/0012-8252(94)90029-9, 1994.

Murphy, M. A., Yin, A., Harrison, T. M., Dürr, S. B., Z, C., Ryerson, F. J., Kidd, W. S. F., X, W., and X, Z.: Did the Indo-Asian collision alone create the Tibetan plateau?, Geology, 25, 719-722, 10.1130/0091-7613(1997)025<0719:Dtiaca>2.3.Co;2, 1997.

Otto, S. C.: Mesozoic-Cenozoic history of deformation and petroleum systems in sedimentary basins of Central Asia; implications of collisions on the Eurasian margin, Petroleum Geoscience, 3, 327-341, 10.1144/petgeo.3.4.327, 1997.

Pearce, J. A.: Geochemical fingerprinting of oceanic basalts with applications to ophiolite classification and the search for Archean oceanic crust, Lithos, 100, 14-48, https://doi.org/10.1016/j.lithos.2007.06.016, 2008.

Pearce, J. A.: Trace element characteristics of lavas from destructive plate boundaries, in: Orogenic Andesites and Related Rocks, edited by: Thorpe,

R. S., John Wiley and Sons, Chichester, England, 525-548, 1982.

Qu, J., Zhang, L., Zhang, J., and Zhang, B.: Petrology and geochronology on high-pressure pelitic granulite from Bulunkuole complex in West Kunlun and its tectonic implication, Acta Petrologica Siniaca, 37, 563-574, 10.18654/1000-0569/2021.02.14, 2021.

Rembe, J., Sobel, E. R., Kley, J., Terbishalieva, B., Musiol, A., Chen, J., and Zhou, R.: Geochronology, Geochemistry, and Geodynamic Implications of Permo-Triassic Back-Arc Basin Successions in the North Pamir, Central Asia, Lithosphere, 2022, 10.2113/2022/7514691, 2022.

Robinson, A. C.: Mesozoic tectonics of the Gondwanan terranes of the Pamir plateau, Journal of Asian Earth Sciences, 102, 170-179, https://doi.org/10.1016/j.jseaes.2014.09.012, 2015.

Robinson, A. C., Yin, A., Manning, C. E., Harrison, T. M., Zhang, S.-H., and Wang, X.-F.: Cenozoic evolution of the eastern Pamir: Implications for strain-accommodation mechanisms at the western end of the Himalayan-Tibetan orogen, GSA Bulletin, 119, 882-896, 10.1130/b25981.1, 2007.

Rollinson, H. R.: Using Geochemical Data: Evaluation, Presentation, Interpretation, Mineralogical Magazine, Longman, Edinburgh Gate, London, 352 pp.1993.

Ruban, D. A., Al-Husseini, M. I., and Iwasaki, Y.: Review of Middle East Paleozoic plate tectonics, GeoArabia, 12, 35-56, 10.2113/geoarabia120335, 2007.

Saktura, W. M., Buckman, S., Nutman, A. P., Walsh, J., and Murray, G.: Magmatic records from the Karakoram terrane: U–Pb zircon ages from granites and modern sediments in the Nubra Valley, NW Himalaya, Journal

of Asian Earth Sciences, 255, 105771, https://doi.org/10.1016/j.jseaes.2023.105771, 2023.

Schwab, M., Ratschbacher, L., Siebel, W., McWilliams, M., Minaev, V., Lutkov, V., Chen, F., Stanek, K., Nelson, B., Frisch, W., and Wooden, J. L.: Assembly of the Pamirs: Age and origin of magmatic belts from the southern Tien Shan to the southern Pamirs and their relation to Tibet, Tectonics, 23, https://doi.org/10.1029/2003TC001583, 2004.

Şengör, A. M. C.: Mid-Mesozoic closure of Permo–Triassic Tethys and its implications, Nature, 279, 590-593, 10.1038/279590a0, 1979.

Şengör, A. M. C.: The Cimmeride Orogenic System and the Tectonics of Eurasia, in: The Cimmeride Orogenic System and the Tectonics of Eurasia, Geological Society of America, 0, 10.1130/SPE195-p1, 1984.

Şengör, A. M. C.: Tectonics of the Tethysides: Orogenic Collage Development in a Collisional Setting, Annual Review of Earth and Planetary Sciences, 15, 213-244, https://doi.org/10.1146/annurev.ea.15.050187.001241, 1987.

Şengör, A. M. C., Altıner, D., Cin, A., Ustaömer, T., and Hsü, K. J.: Origin and assembly of the Tethyside orogenic collage at the expense of Gondwana Land, Geological Society, London, Special Publications, 37, 119-181, doi:10.1144/GSL.SP.1988.037.01.09, 1988.

Sobel, E. R.: Basin analysis of the Jurassic–Lower Cretaceous southwest Tarim basin, northwest China, GSA Bulletin, 111, 709-724, 10.1130/0016-7606(1999)111<0709:Baotjl>2.3.Co;2, 1999.

Sobel, E. R., Chen, J., Schoenbohm, L. M., Thiede, R., Stockli, D. F., Sudo, M., and Strecker, M. R.: Oceanic-style subduction controls late Cenozoic deformation of the Northern Pamir orogen, Earth and Planetary Science

Letters, 363, 204-218, https://doi.org/10.1016/j.epsl.2012.12.009, 2013.

Stampfli, G., Marcoux, J., and Baud, A.: Tethyan margins in space and time, Palaeogeography, Palaeoclimatology, Palaeoecology, 87, 373-409, https://doi.org/10.1016/0031-0182(91)90142-E, 1991.

Stampfli, G. M.: Tethyan oceans, Geological Society, London, Special Publications, 173, 1-23, doi:10.1144/GSL.SP.2000.173.01.01, 2000.

Stampfli, G. M. and Borel, G. D.: A plate tectonic model for the Paleozoic and Mesozoic constrained by dynamic plate boundaries and restored synthetic oceanic isochrons, Earth and Planetary Science Letters, 196, 17-33, https://doi.org/10.1016/S0012-821X(01)00588-X, 2002.

Sun, S.-S. and McDonough, W. F.: Chemical and isotopic systematics of oceanic basalts: implications for mantle composition and processes, Geological Society, London, Special Publications, 42, 313-345, doi:10.1144/GSL.SP.1989.042.01.19, 1989.

Tapponnier, P., Mattauer, M., Proust, F., and Cassaigneau, C.: Mesozoic ophiolites, sutures, and arge-scale tectonic movements in Afghanistan, Earth and Planetary Science Letters, 52, 355-371, https://doi.org/10.1016/0012-821X(81)90189-8, 1981.

Tao, Z., Yin, J., Spencer, C. J., Sun, M., Xiao, W., Kerr, A. C., Wang, T., Huangfu, P., Zeng, Y., and Chen, W.: Subduction polarity reversal facilitated by plate coupling during arc-continent collision: Evidence from the Western Kunlun orogenic belt, northwest Tibetan Plateau, Geology, 10.1130/g51847.1, 2024.

Vermeesch, P.: IsoplotR: A free and open toolbox for geochronology, Geoscience Frontiers, 9, 1479-1493,

https://doi.org/10.1016/j.gsf.2018.04.001, 2018.

Vermeesch, P.: On the visualisation of detrital age distributions, Chemical Geology, 312-313, 190-194, https://doi.org/10.1016/j.chemgeo.2012.04.021, 2012.

Wan, B., Chu, Y., Chen, L., Zhang, Z., Ao, S., and Talebian, M.: When and Why the NeoTethyan Subduction Initiated Along the Eurasian Margin, in: Compressional Tectonics, 245-260, https://doi.org/10.1002/9781119773856.ch9, 2023.

Wan, B., Wu, F., Chen, L., Zhao, L., Liang, X., Xiao, W., and Zhu, R.: Cyclical one-way continental rupture-drift in the Tethyan evolution: Subduction-driven plate tectonics, Science China Earth Sciences, 62, 2005-2016, 10.1007/s11430-019-9393-4, 2019.

Wang, C., Ding, L., Zhang, L.-Y., Kapp, P., Pullen, A., and Yue, Y.-H.: Petrogenesis of Middle–Late Triassic volcanic rocks from the Gangdese belt, southern Lhasa terrane: Implications for early subduction of Neo-Tethyan oceanic lithosphere, Lithos, 262, 320-333, https://doi.org/10.1016/j.lithos.2016.07.021, 2016.

Wang, Y., Qian, X., Cawood, P. A., Liu, H., Feng, Q., Zhao, G., Zhang, Y., He, H., and Zhang, P.: Closure of the East Paleotethyan Ocean and amalgamation of the Eastern Cimmerian and Southeast Asia continental fragments, Earth-Science Reviews, 186, 195-230, https://doi.org/10.1016/j.earscirev.2017.09.013, 2018.

Wei, Y., Zhao, Z., Niu, Y., Zhu, D.-C., Liu, D., Wang, Q., Hou, Z., Mo, X., and Wei, J.: Geochronology and geochemistry of the Early Jurassic Yeba Formation volcanic rocks in southern Tibet: Initiation of back-arc rifting and

crustal accretion in the southern Lhasa Terrane, Lithos, 278-281, 477-490, https://doi.org/10.1016/j.lithos.2017.02.013, 2017.

Weller, O. M., Mottram, C. M., St-Onge, M. R., Möller, C., Strachan, R., Rivers, T., and Copley, A.: The metamorphic and magmatic record of collisional orogens, Nature Reviews Earth & Environment, 2, 781-799, 10.1038/s43017-021-00218-z, 2021.

Winchester, J. A. and Floyd, P. A.: Geochemical discrimination of different magma series and their differentiation products using immobile elements, Chemical Geology, 20, 325-343, https://doi.org/10.1016/0009-2541(77)90057-2, 1977.

Wu, C., Yin, A., Zuza, A. V., Zhang, J., Liu, W., and Ding, L.: Pre-Cenozoic geologic history of the central and northern Tibetan Plateau and the role of Wilson cycles in constructing the Tethyan orogenic system, Lithosphere, 8, 254-292, 10.1130/l494.1, 2016.

Wu, F. Y., Wan, B., Zhao, L., Xiao, W. J., and Zhu, R. X.: Tethyan geodynamics, Acta Petrologica Siniaca, 36, 1627-1674, 2020.

Wu, H., Cheng, X., Chen, H., Chen, C., Dilek, Y., Shi, J., Zeng, C., Li, C., Zhang, W., Zhang, Y., Lin, X., and Zhang, F.: Tectonic Switch From Triassic Contraction to Jurassic-Cretaceous Extension in the Western Tarim Basin, Northwest China: New Insights Into the Evolution of the Paleo-Tethyan Orogenic Belt, Frontiers in Earth Science, 9, 10.3389/feart.2021.636383, 2021.

Xiao, W. J., Windley, B. F., Chen, H. L., Zhang, G. C., and Li, J. L.: Carboniferous-Triassic subduction and accretion in the western Kunlun, China: Implications for the collisional and accretionary tectonics of the

northern Tibetan Plateau, Geology, 30, 295-298, 10.1130/0091-7613(2002)030<0295:Ctsaai>2.0.Co;2, 2002.

Xiao, W. J., Windley, B. F., Liu, D. Y., Jian, P., Liu, C. Z., Yuan, C., and Sun, M.: Accretionary Tectonics of the Western Kunlun Orogen, China: A Paleozoic–Early Mesozoic, Long‐Lived Active Continental Margin with Implications for the Growth of Southern Eurasia, The Journal of Geology, 113, 687-705, 10.1086/449326, 2005.

Xie, F. and Tang, J.: The Late Triassic-Jurassic magmatic belt and its implications for the double subduction of the Neo-Tethys Ocean in the southern Lhasa subterrane, Tibet, Gondwana Research, 97, 1-21, https://doi.org/10.1016/j.gr.2021.05.007, 2021.

Xie, Y. and Dilek, Y.: Detrital zircon U–Pb geochronology and fluvial basin evolution of the Liuqu Conglomerate within the Yarlung Zangbo Suture Zone: A critical geochronometer for the collision tectonics of the Tibetan-Himalayan Orogenic Belt, Geosystems and Geoenvironment, 2, 100178, https://doi.org/10.1016/j.geogeo.2023.100178, 2023.

Xu, W., Zhao, Z., and Dai, L.: Post-collisional mafic magmatism: Record of lithospheric mantle evolution in continental orogenic belt, Science China Earth Sciences, 63, 2029-2041, 10.1007/s11430-019-9611-9, 2020.

Yan, J.: The early Paleozoic tectono-sedimentary characteristics and the basin-orogen process in south Tarim Basin, School of Earth Sciences, Zhejiang University, Hangzhou, Zhejiang, China, 137 pp., 10.27461/d.cnki.gzjdx.2022.002783, 2022 (in Chinese with English abstract).

Yang, Y.-T., Guo, Z.-X., and Luo, Y.-J.: Middle-Late Jurassic

tectonostratigraphic evolution of Central Asia, implications for the collision of the Karakoram-Lhasa Block with Asia, Earth-Science Reviews, 166, 83-110, https://doi.org/10.1016/j.earscirev.2017.01.005, 2017.

Zhang, K.-J., Zhang, Y.-X., Tang, X.-C., and Xia, B.: Late Mesozoic tectonic evolution and growth of the Tibetan plateau prior to the Indo-Asian collision, Earth-Science Reviews, 114, 236-249, https://doi.org/10.1016/j.earscirev.2012.06.001, 2012.

Zhang, Q., Wu, Z., Chen, X., Zhou, Q., and Shen, N.: Proto-Tethys oceanic slab break-off: Insights from early Paleozoic magmatic diversity in the West Kunlun Orogen, NW Tibetan Plateau, Lithos, 346-347, 105147, https://doi.org/10.1016/j.lithos.2019.07.014, 2019a.

Zhang, S., Hu, X., and Garzanti, E.: Paleocene initial indentation and early growth of the Pamir as recorded in the western Tarim Basin, Tectonophysics, 772, 228207, https://doi.org/10.1016/j.tecto.2019.228207, 2019b.

Zhang, Z., Xiao, W., Ji, W., Majidifard, M. R., Rezaeian, M., Talebian, M., Xiang, D., Chen, L., Wan, B., Ao, S., and Esmaeili, R.: Geochemistry, zircon U-Pb and Hf isotope for granitoids, NW Sanandaj-Sirjan zone, Iran: Implications for Mesozoic-Cenozoic episodic magmatism during Neo-Tethyan lithospheric subduction, Gondwana Research, 62, 227-245, https://doi.org/10.1016/j.gr.2018.04.002, 2018.

Zhao, G., Wang, Y., Huang, B., Dong, Y., Li, S., Zhang, G., and Yu, S.: Geological reconstructions of the East Asian blocks: From the breakup of Rodinia to the assembly of Pangea, Earth-Science Reviews, 186, 262-286, https://doi.org/10.1016/j.earscirev.2018.10.003, 2018.

Zhao, J., Zeng, X., Tian, J., Hu, C., Wang, D., Yan, Z., Wang, K., and Zhao, X.: Provenance and paleogeography of the Jurassic Northwestern Qaidam Basin (NW China): Evidence from sedimentary records and detrital zircon geochronology, Journal of Asian Earth Sciences, 190, 104060, https://doi.org/10.1016/j.jseaes.2019.104060, 2020.

Zhao, Z.-F., Dai, L.-Q., and Zheng, Y.-F.: Postcollisional mafic igneous rocks record crust-mantle interaction during continental deep subduction, Scientific Reports, 3, 3413, 10.1038/srep03413, 2013.

Zheng, Y., Mao, J., Chen, Y., Sun, W., Ni, P., and Yang, X.: Hydrothermal ore deposits in collisional orogens, Science Bulletin, 64, 205-212, https://doi.org/10.1016/j.scib.2019.01.007, 2019.

Zhou, C.-A., Song, S., Allen, M. B., Wang, C., Su, L., and Wang, M.: Post-collisional mafic magmatism: Insights into orogenic collapse and mantle modification from North Qaidam collisional belt, NW China, Lithos, 398-399, 106311, https://doi.org/10.1016/j.lithos.2021.106311, 2021.

Zhou, N., Chen, B., Deng, Z., Sang, M., and Bai, Q.: Discovery and Significance of Early Jurassic Bimodal Volcanic Rocks in Huoshaoyun, Karakoram, Geoscience, 33, 990-1002, 10.19657/j.geoscience.1000-8527.2019.05.06, 2019 (in Chinese with English abstract).

Zhu, D.-C., Wang, Q., Cawood, P. A., Zhao, Z.-D., and Mo, X.-X.: Raising the Gangdese Mountains in southern Tibet, Journal of Geophysical Research: Solid Earth, 122, 214-223, https://doi.org/10.1002/2016JB013508, 2017.

Zhu, R., Zhao, P., and Zhao, L.: Tectonic evolution and geodynamics of the Neo-Tethys Ocean, Science China Earth Sciences, 65, 1-24, 10.1007/s11430-021-9845-7, 2022.

1275 Zuza, A. V. and Yin, A.: Balkatach hypothesis: A new model for the evolution of
1276 the Pacific, Tethyan, and Paleo-Asian oceanic domains, Geosphere, 13,
1277 1664-1712, 10.1130/ges01463.1, 2017.
1278

Supplementary Materials

Table S1: Analytical methodology.

Table S2: Zircon U-Pb data of Jurassic basalt and sedimentary rocks.

Table S3: Trace element of zircons.

Table S4: Jurassic conglomerate clast lithologies.

Table S5: Whole rock geochemical results of Jurassic basalts.

Fig. S1: Correlations between the trace elements of Jurassic basalts.

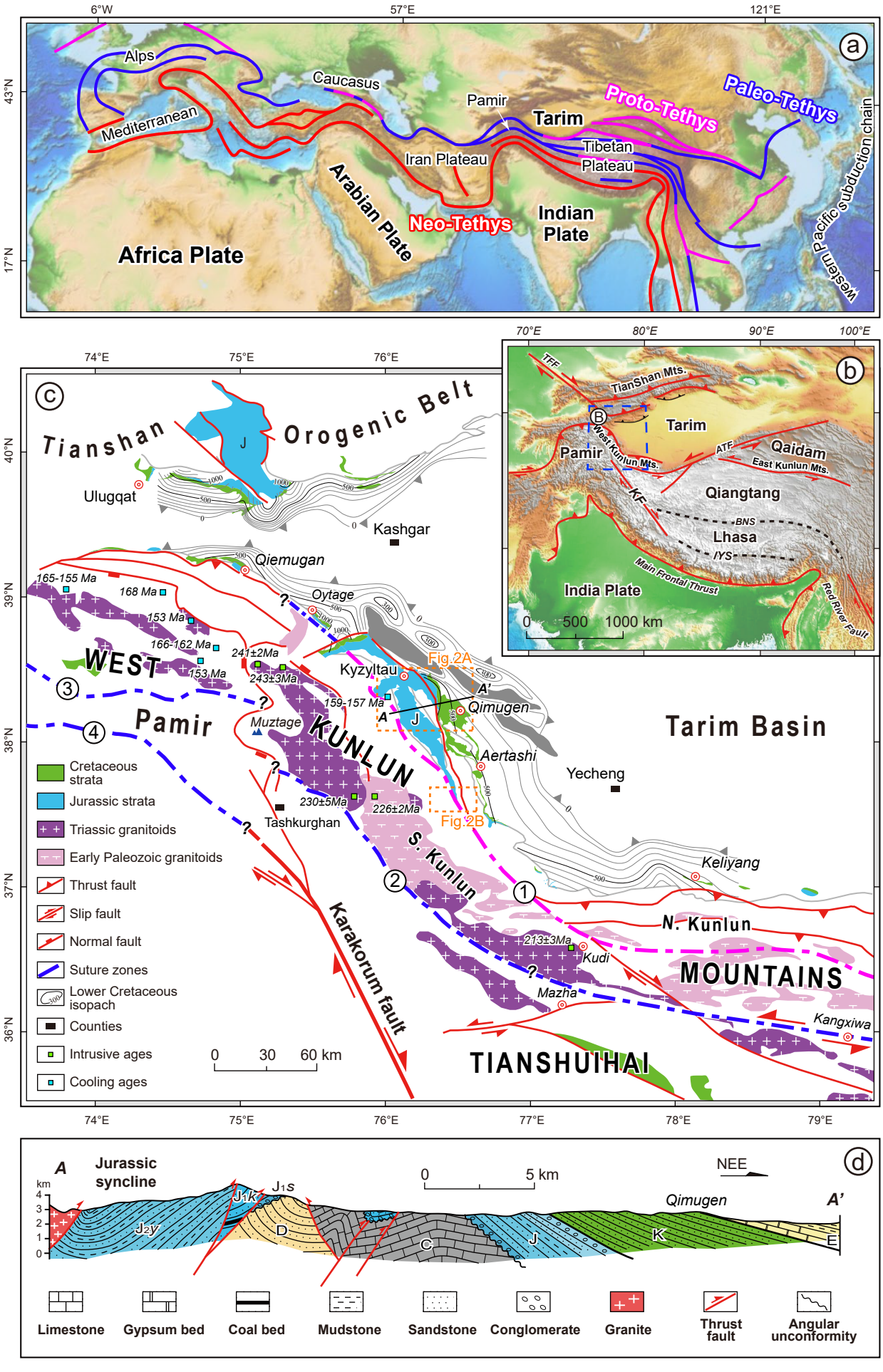
a
Alps
Caucasus
Mediterranean
Pamir
Tarim
Proto-Tethys
Paleo-Tethys
Tibetan Plateau
Iran Plateau
Arabian Plate
Neo-Tethys
Indian Plate
Africa Plate
Western Pacific subduction chain
b
TFF
TianShan Mts.
Tarim
Pamir
West Kunlun Mts.
ATF
Qaidam
East Kunlun Mts.
KF
Qiangtang
BNS
Lhasa
IYS
Main Frontal Thrust
India Plate
Red River Fault
0 500 1000 km
c
Tianshan Orogenic Belt
Ulugqat
Kashgar
Qiemugan
Oytage
Kyzyltau
Qimugen
Aertashi
Yecheng
Keliyang
Muztage
Tashkurghan
WEST Pamir
KUNLUN
S. Kunlun
N. Kunlun MOUNTAINS
Karakorum fault
TIANSHUIHAI
Tarim Basin
165-155 Ma
168 Ma
153 Ma
166-162 Ma
153 Ma
241±2Ma
243±3Ma
159-157 Ma
230±5Ma
226±2Ma
213±3Ma
Kudi
Mazha
Kangxiwa
Fig.2A
Fig.2B
Cretaceous strata
Jurassic strata
Triassic granitoids
Early Paleozoic granitoids
Thrust fault
Slip fault
Normal fault
Suture zones
Lower Cretaceous isopach
Counties
Intrusive ages
Cooling ages
0 30 60 km
d
A
Jurassic syncline
km
J1s
J1k
J2y
D
C
J
K
E
Qimugen
A'
NEE
0 5 km
Limestone
Gypsum bed
Coal bed
Mudstone
Sandstone
Conglomerate
Granite
Thrust fault
Angular unconformity

Figure 1 (a) Tectonic plate framework in the Northern Hemisphere and the suture zones within the Tethyan Realm (modified from Wu et al., 2020); (b) Structural framework of central Asia showing main blocks and orogenic belts, with locations of major sutures and boundary faults: TFF-Talas-Fergana Fault, BNS-Bangong-Nujiang suture, IYS-Indus-Yalu suture, ATF-Altyn-Tage Fault; (c) Simplified geologic map of the Western Kunlun Mountains including major units and suture zones (modified from Wu et al., 2021; cooling ages of basements refer to Yang et al., 2017): ①- Early Paleozoic Kudi suture, ②- Triassic Mazar-Kangxiwa suture, ③- Triassic Tanymas suture separating the North and Central Pamirs, ④- Rushan-Pshart zone separating the Central and South Pamirs; (d) A section across the east part of the Western Kunlun Mountains showing the deformed and fragmented Jurassic basin. The section location is presented in Fig.1 (c).

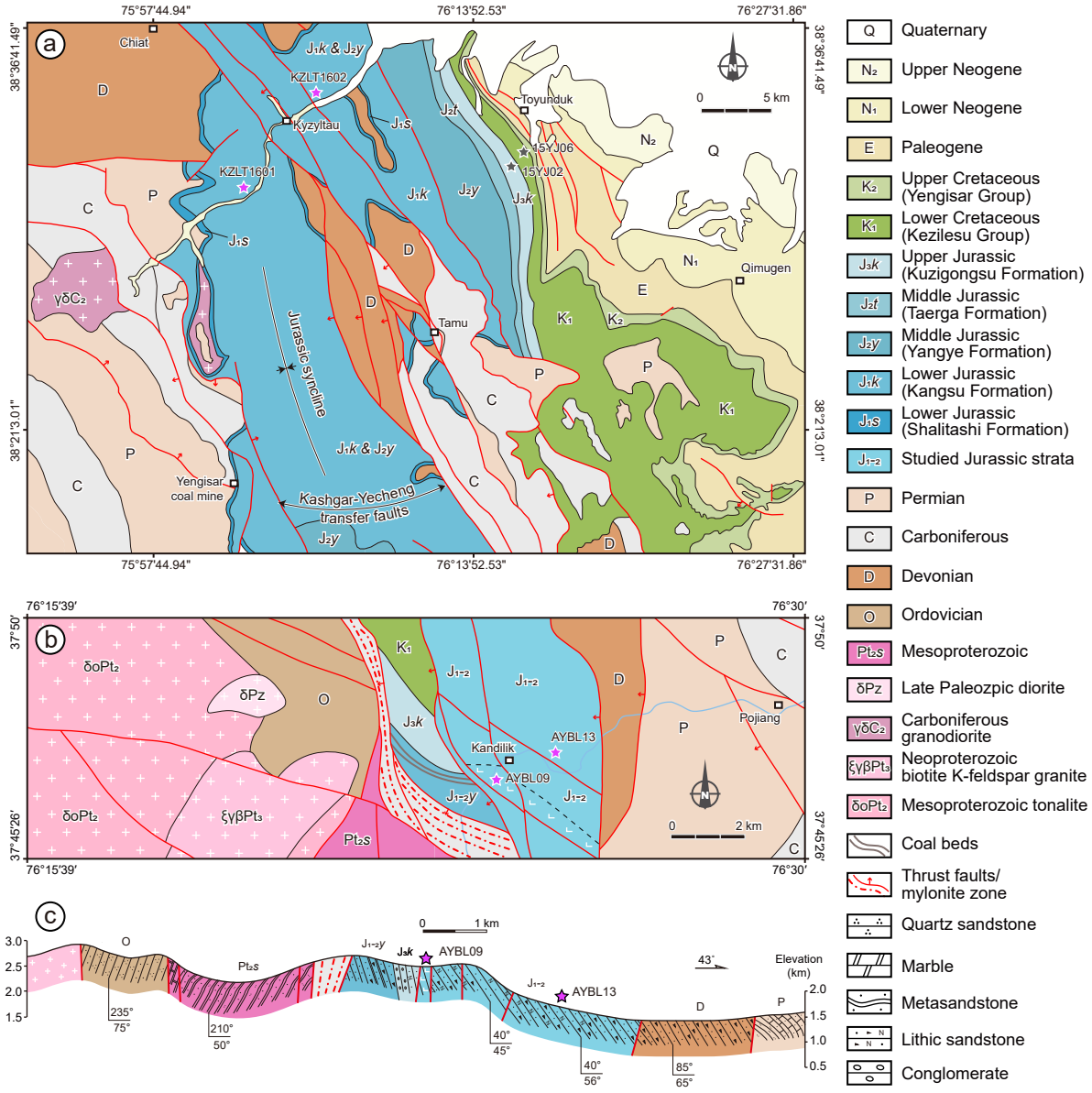

Figure 2 (a) Geological map in the Kyzyltau region showing the stratigraphic information and sampling locations; (b) Geological map in the Kandilik region showing the Proterozoic basements and Paleozoic-Mesozoic strata. The red stars mark sampling locations in this work, and the grey stars mark the locations of published data (Zhang et al., 2019b); (c) A field geological section showing the regional strata and deformation along the Pojiang River in Fig. 2b.

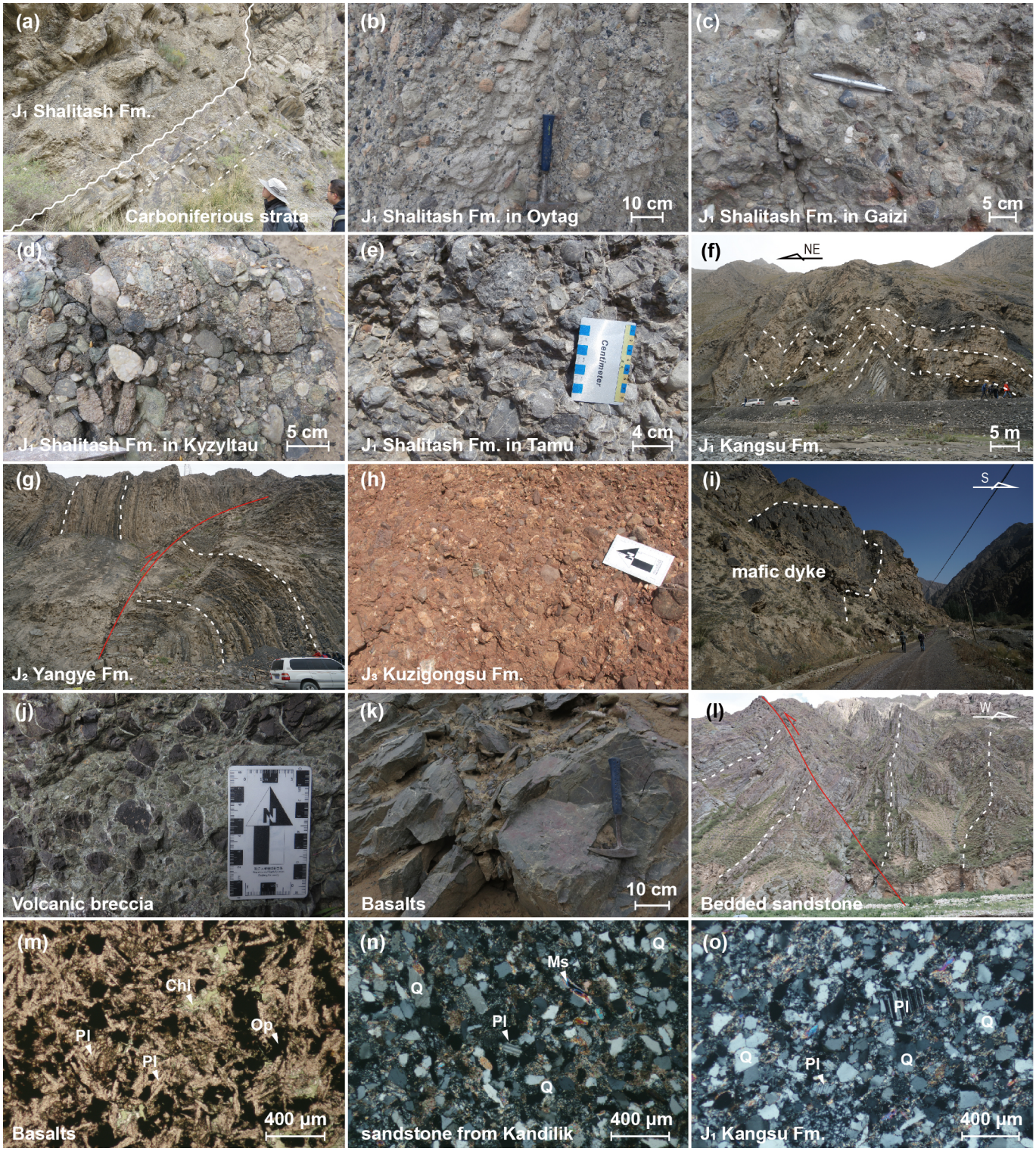

Figure 3 Photographs showing the observation from field and binocular microscope. (a) Early Jurassic Shalitash Formation overlying on the deformed Carboniferous strata with angular unconformity; (b) Conglomerate clast lithologies of the Shalitash Formation in Oytag, (c) Gaizi; (d) Kyzyltau and (e) Tamu; (f) Early Jurassic Kangsu Formation with strongly deformed sandstone layers; (g) Strong deformation of the turbidite sequences in the Middle Jurassic Yangye Formation; (h) Conglomerate clast lithologies in the Late Jurassic Kuzigongsu Formation; (i) Mafic dyke within newly identified Jurassic strata in the Kandilik region; (j) Basaltic volcanic breccia; (k) Massive basalt layer; (l) Jurassic bedded feldspar lithic sandstones with great thickness, which was previously assigned to be Precambrian age; (m) Micrograph of basalt under plane-polarized light; (n) Micrograph of Jurassic sandstone under cross-polarized light from Kandilik section; (o) Micrograph of Jurassic sandstone under cross-polarized light from Kyzyltau section.

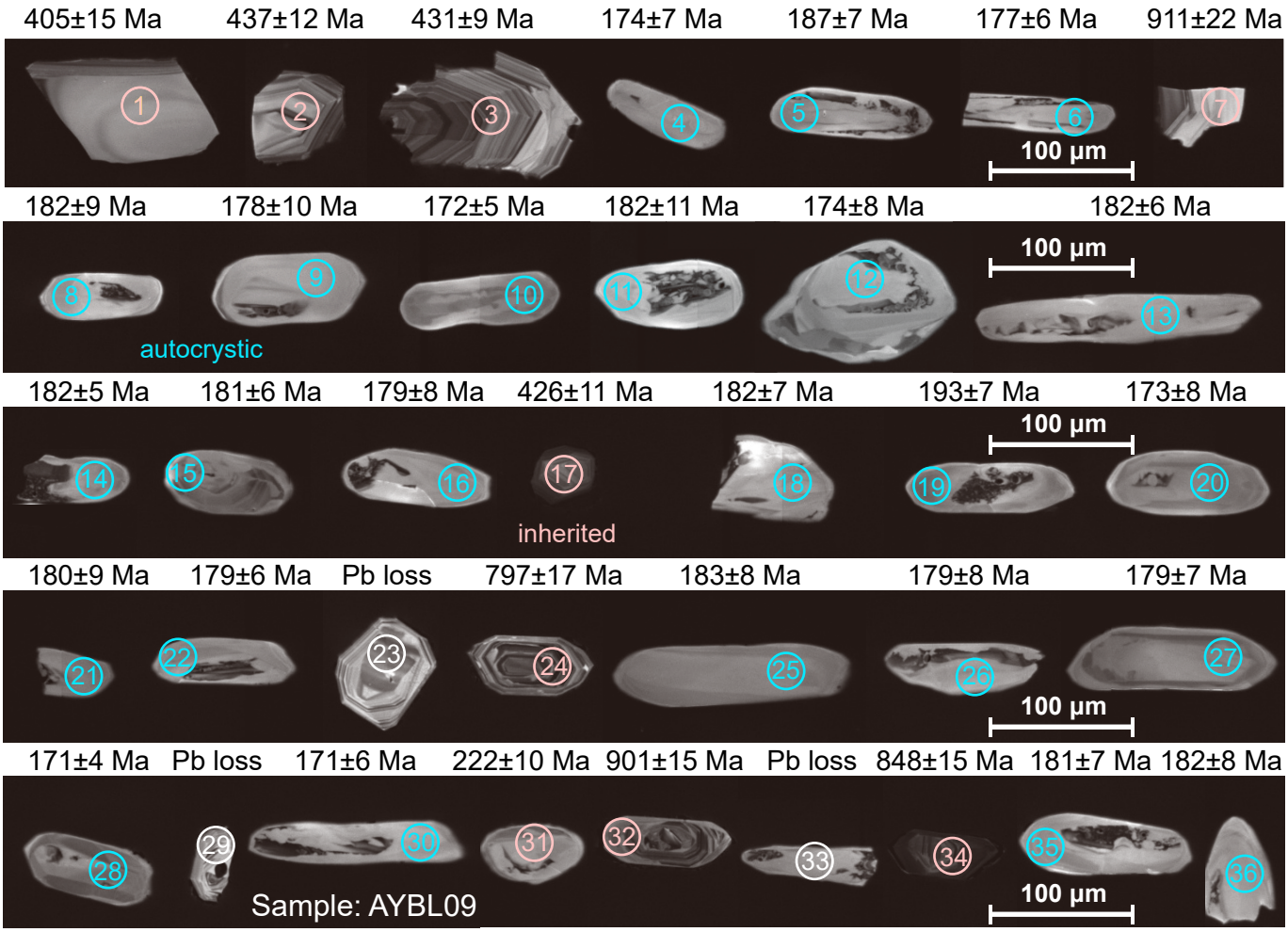

Figure 4 CL images of all tested zircon varieties in basalt sample AYBL09, noting the apparent $^{206}Pb/^{238}U$ ages above. The red circle indicates the target points of type 1 zircon, the blue circle represents the target points of type 2 zircon, and the white circle marks the points where discordant ages were obtained.

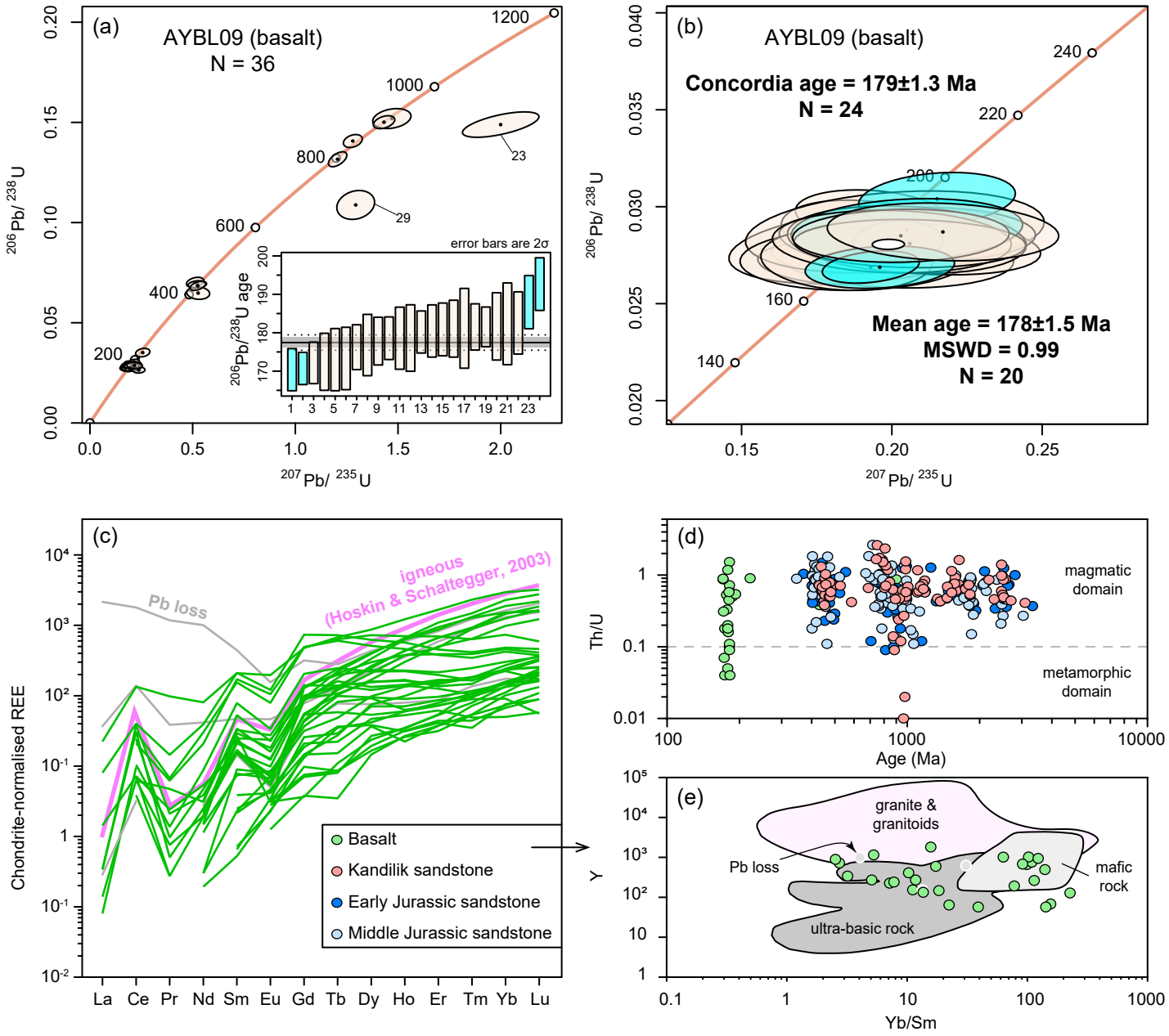

Figure 5 (a) Concordia plot of LA-ICP-MS U-Pb analysis for the zircons of the basalt sample AYBL09; (b) Weighted mean $^{206}Pb/^{238}U$ age and concordia age of the youngest zircon groups; (c) Zircon chondrite-normalised REE pattern of the basalt; (d) Th/U ratios of zircons from basalt and sandstone samples. (e) Yb/Sm-Y plotting to distinguish the origins of zircons from the basalt.

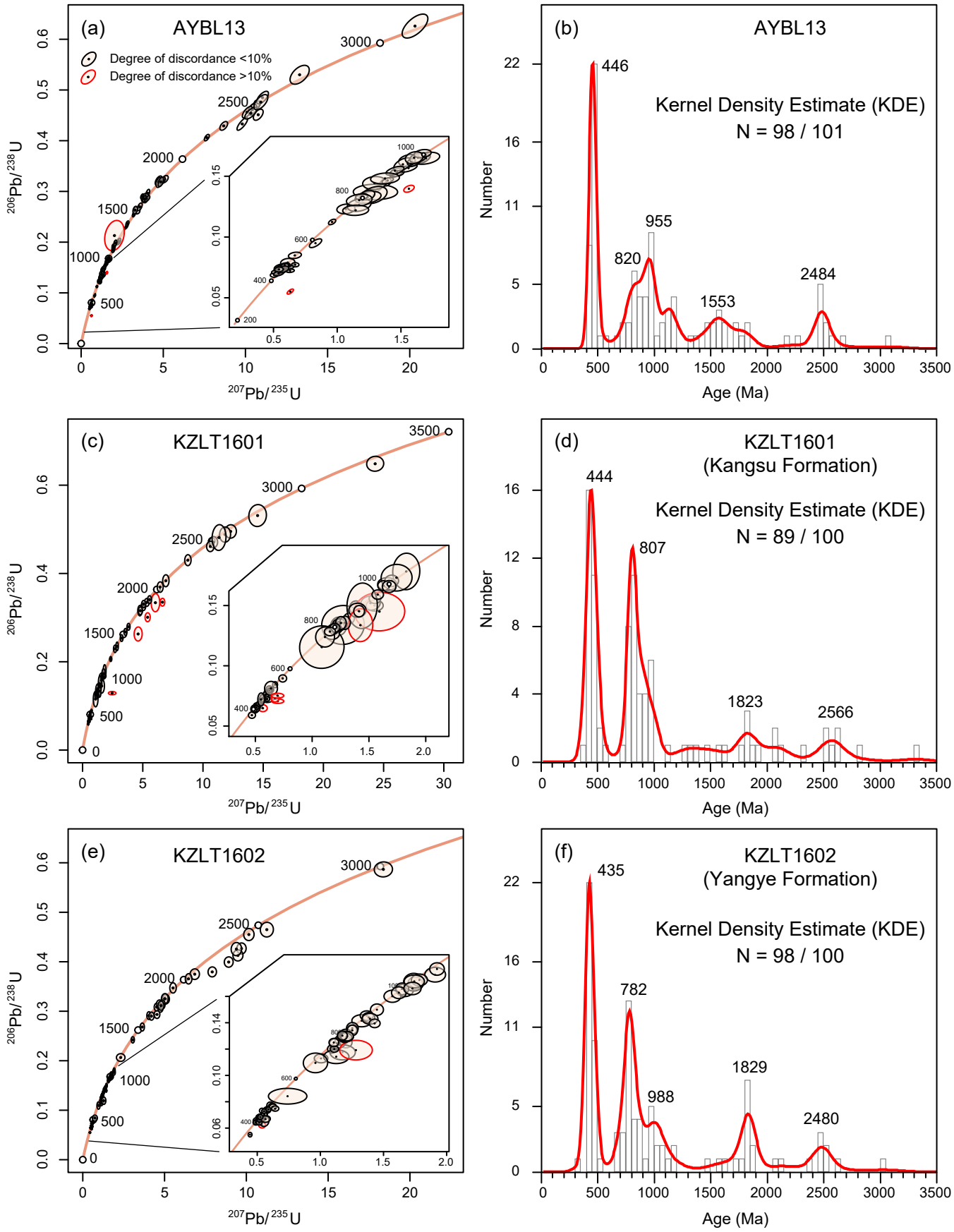

Figure 6 Concordia diagram for the detrital zircons of (a) sample AYBL13 from Kandilik section, (c) sample KZLT1601 from Kangsu Formation, and (e) sample KZLT1602 from Yangye Formation; Diagram of the Kernel Density Estimate of detrital zircon U-Pb ages for (b) AYBL13, (d) KZLT1601, and (f) KZLT1602.

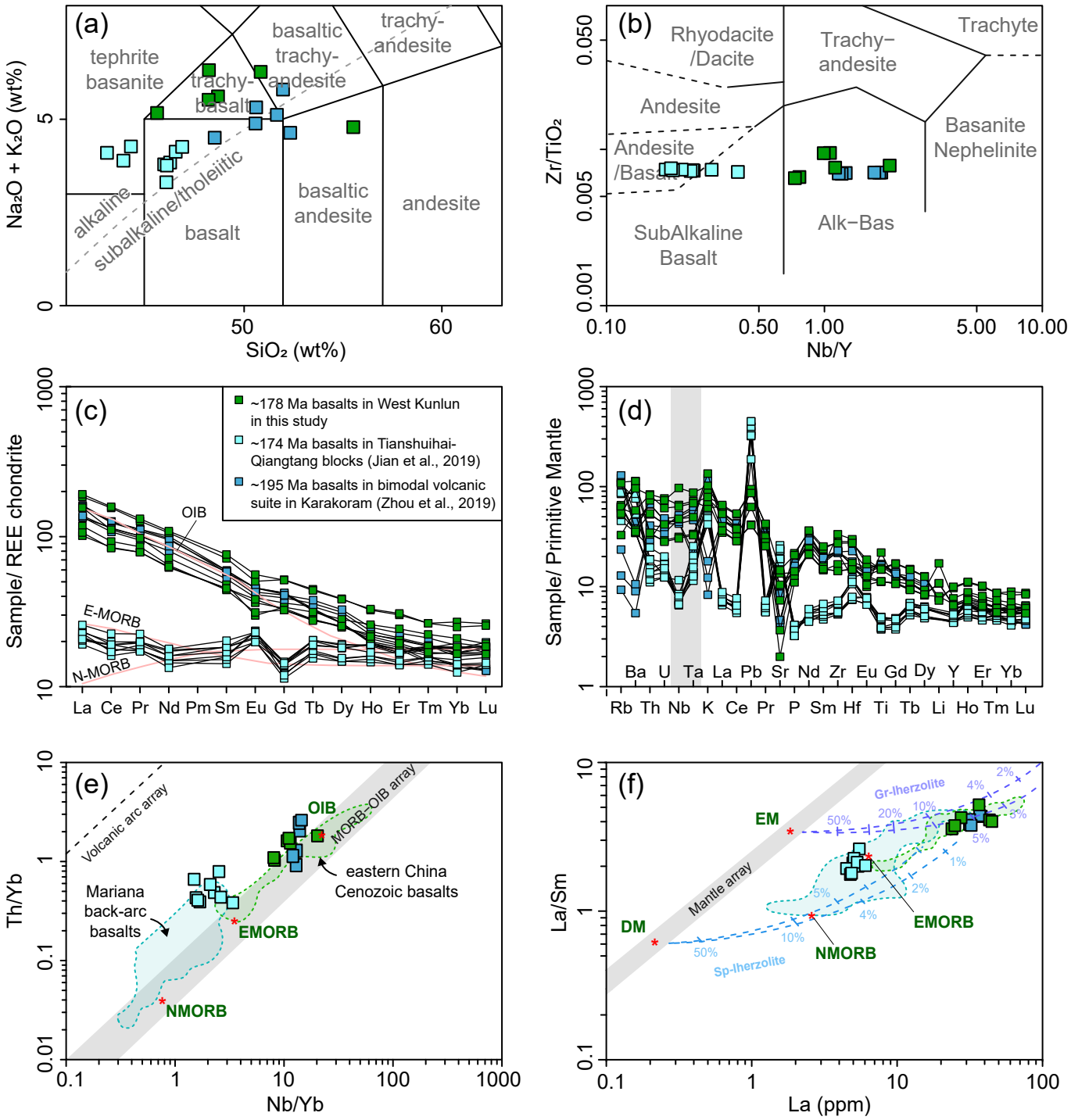

Figure 7 Geochemical classification diagram of Jurassic basalt samples from the Kandilik region in the West Kunlun Mountains (green) and from Longshan Formation in the Tianshuihai terrane (blue): (a) total alkali versus silica (Middlemost, 1994) and (b) Zr/TiO_2 vs. Nb/Y diagrams (Winchester and Floyd, 1977); (c) Rare earth elements pattern (REE) and (d) trace element diagrams of Jurassic basalts; (e) Th/Yb vs. Nb/Yb plot (Pearce, 2008) and (f) La/Sm vs. La plot (Aldanmaz et al., 2000) Chondrite-normalized REE and the primitive mantle-normalized values refer to Sun and McDonough (1989). The range of the Mariana back-arc basalts refers to Pearce (2008) and the range of eastern China Cenozoic basalts refers to Guo et al. (2020).

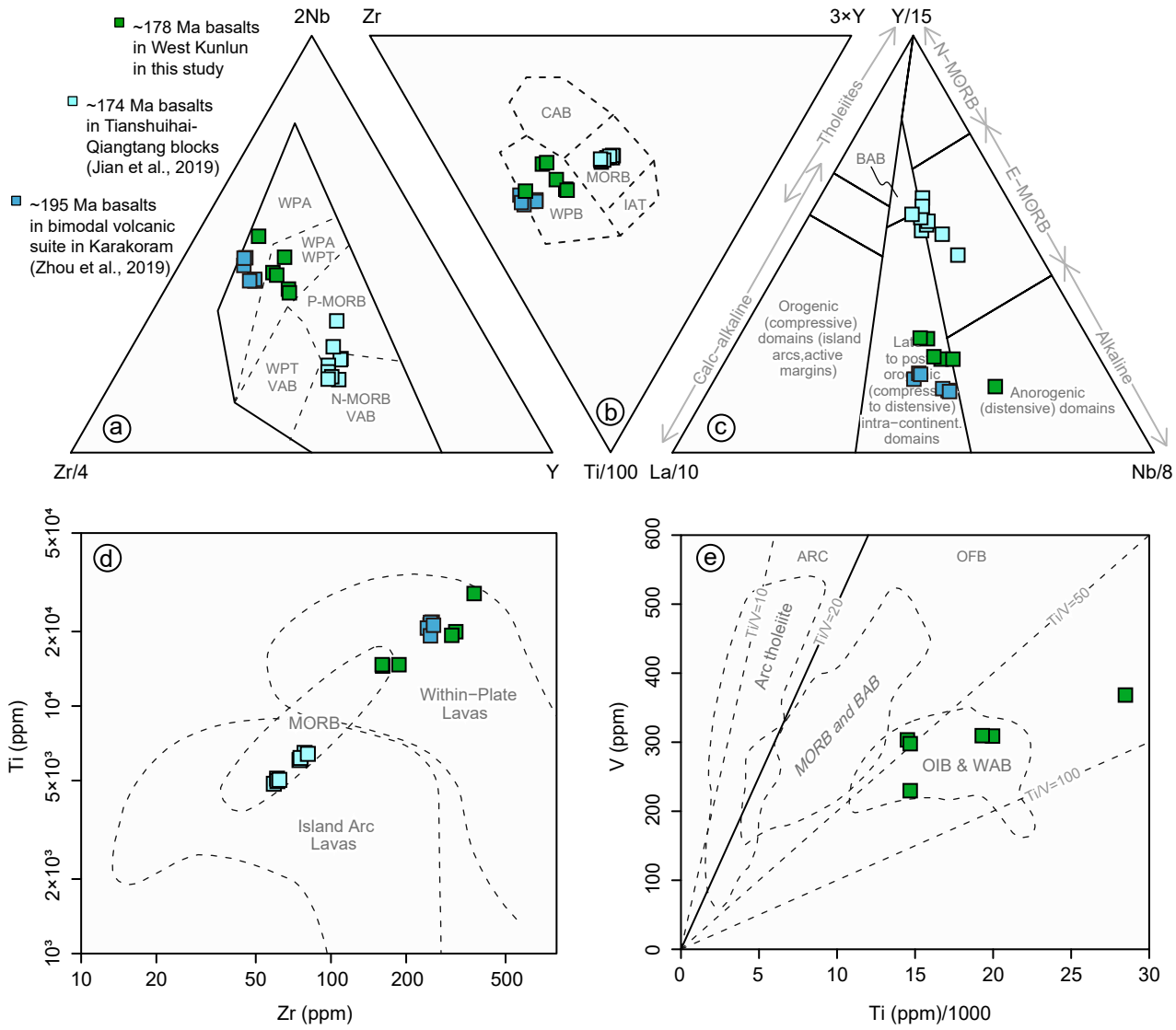

Figure 8 Tectonic discrimination diagrams for Jurassic basalts through (a) Zr/4-2Nb-Y plot and (b) Zr-3Y-Ti/100 plot (Meschede, 1986), (c) La/10-Y/15-Nb/8 plot (Cabanis and Lecolle, 1989), (d) Ti-Zr plot (Pearce, 1982) and (d) V-Ti/1000 plot (Rollinson, 1993). Abbreviation: WPB-within plate basalts; WPA- within plate alkali basalts; WPT-within plate tholeiites; VAB-volcanic arc basalts; CAB- calc-alkali basalts; IAT-island arc tholeiites; BAB-back arc basalts.

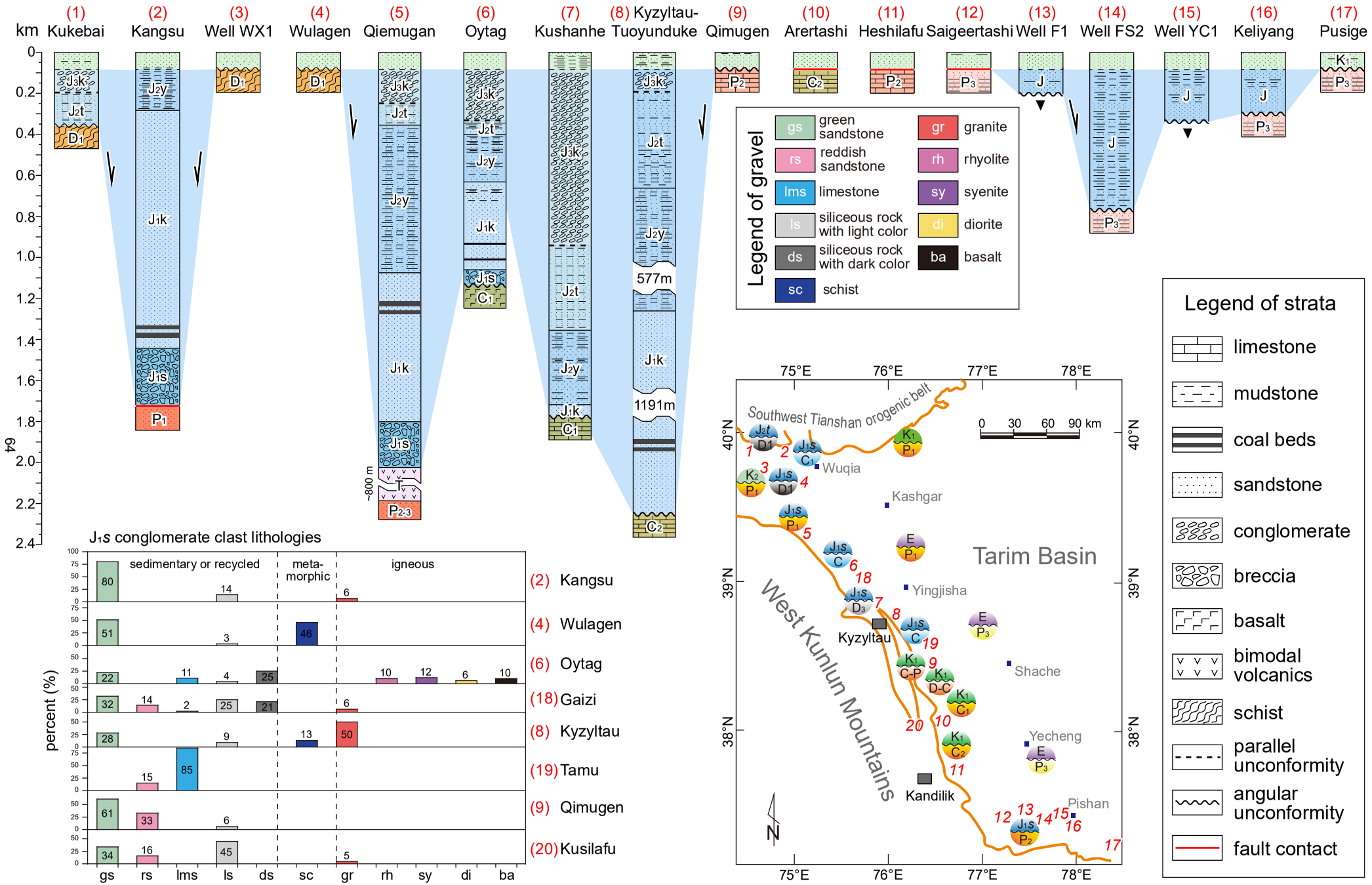

Figure 9 Stratigraphic correlations of Jurassic basin along east flank of the Western Kunlun Mountains (modified from Wu et al., 2021 and Rembe et al., 2022) and the results of gravel analysis of Early Jurassic conglomerate.

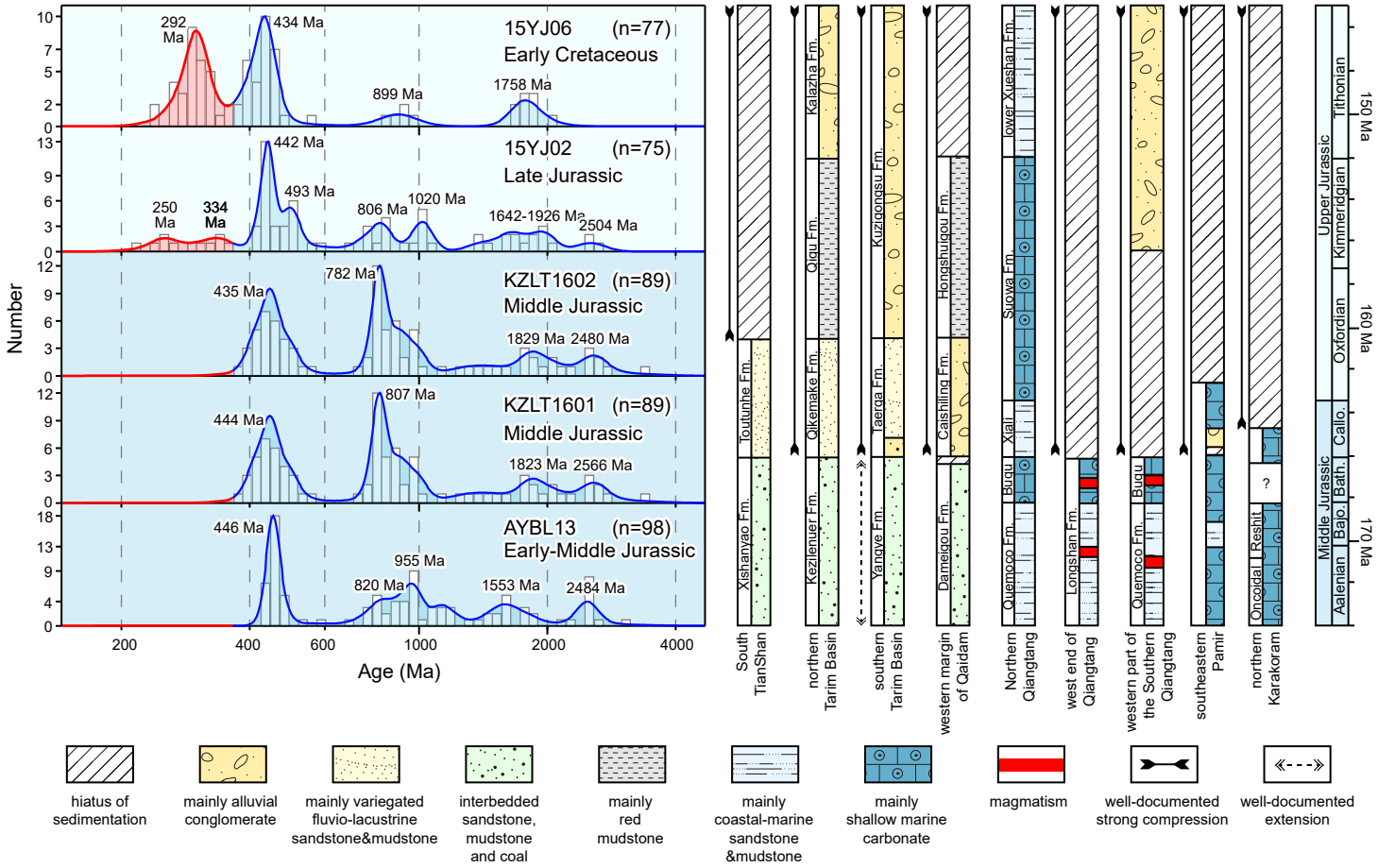

Figure 10 Late Jurassic basin inversion based on the provenance variation through the Early Jurassic to Early Cretaceous and the stratigraphic correlation in the northwestern China. Late Jurassic and Early Cretaceous sandstone samples are according to Zhang et al. (2019b). The sampling locations are shown in Fig. 2a. Stratigraphic correlation is modified from Yang et al. (2017).

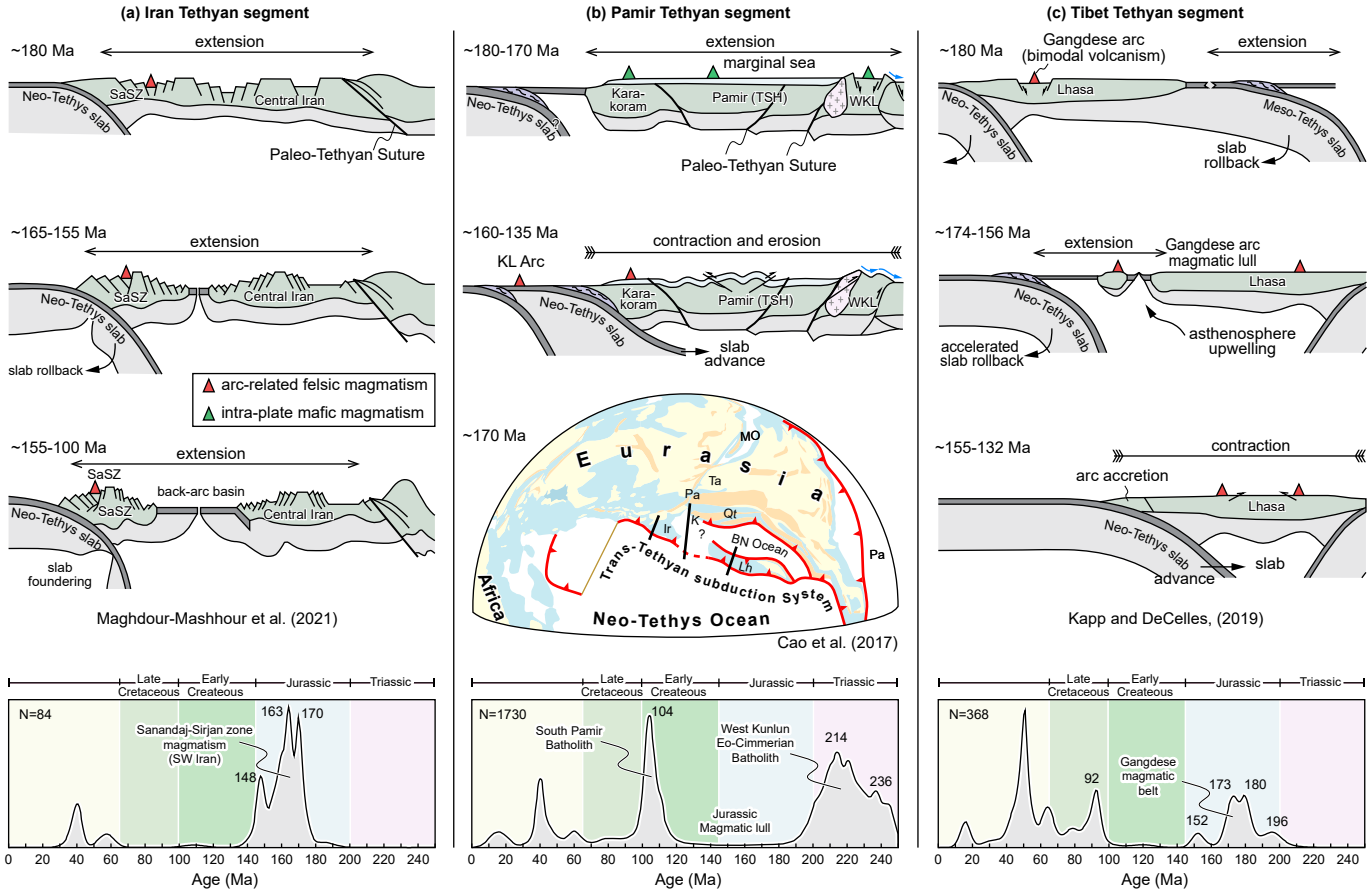

Figure 11 Illustrative cartoons indicating the tectonic variation of the southern Eurasian margin in Jurassic. The subduction of the Neo-Tethys Ocean resulted in persistent rifting along the Iran Tethyan segment, generating massive magmatism during the Early Jurassic to Early Cretaceous. The far-field subduction causing the Early-Middle Jurassic extension along the Pamir Tethyan segment without magmatic flare-up. The changes in subduction style along the Pamir and Tibet Tethyan segments induced the extension-contraction transition. The spatial magmatic datasets are according to Zhang et al. (2018), Chapman et al. (2018), Ma et al. (2017b) and Zhu et al. (2017), and the map of paleogeographic reconstruction is modified from Cao et al. (2017). Abbreviation: SaSZ- Sanandaj-Sirjan zone; TSH-Tianshuihai block; WKL-West Kunkun Mountains; KL Arc- Kohistan Ladakh Arc; Ir-Iran; K-Karakoram; Pa-Pamir; Ta-Tarim; Qt-Qiangtang; Lh-Lhasa; BN Ocean-Bangong-Nujiang Ocean.